Sensitivity of clumped isotope temperatures in fossil benthic and planktic foraminifera to diagenetic alteration

Thomas J. Leutert [a,*], Philip F. Sexton [b], Aradhna Tripati [c,d], Alison Piasecki [a,e]
Sze Ling Ho [a,f], A. Nele Meckler [a]

[a] *Bjerknes Centre for Climate Research and Department of Earth Science, University of Bergen, 5007 Bergen, Norway*
[b] *School of Environment, Earth & Ecosystem Sciences, The Open University, Milton Keynes MK7 6AA, UK*
[c] *Department of Earth, Planetary, and Space Sciences, Department of Atmospheric and Oceanic Sciences, Institute of the Environment and Sustainability, Center for Diverse Leadership in Science, University of California, Los Angeles, CA 90095, USA*
[d] *European Institute of Marine Sciences (IUEM), Université de Brest, UMR 6538, Domaines Océaniques, Rue Dumont D'Urville, and IFREMER, Laboratoire Géophysique et enregistrement Sédimentaire, 29280 Plouzané, France*
[e] *Department of Earth and Planetary Sciences, Harvard University, Cambridge, MA 02138, USA*
[f] *Institute of Oceanography, National Taiwan University, 10617 Taipei, Taiwan*

Abstract

Applying the clumped isotope (Δ_{47}) thermometer to foraminifer microfossils offers the potential to significantly improve paleoclimate reconstructions, owing to its insensitivity to the isotopic composition of seawater (unlike traditional oxygen isotope ($\delta^{18}O$) analyses). However, the extent to which primary Δ_{47} signatures of foraminiferal calcites can be altered during diagenesis is not well known. Here, we present Δ_{47} data as well as high-resolution (~10 kyr) $\delta^{18}O$ and $\delta^{13}C$ middle Eocene time series, measured on benthic and planktic foraminifera from ODP/IODP Sites 1408, 1409, 1410, 1050, 1260 and 1263 in the Atlantic Ocean. The sites examined span various oceanographic regimes, including the western tropical to mid-latitude North Atlantic, and the eastern mid-latitude South Atlantic. Comparing data from contemporaneous foraminifera with different preservation states, we test the effects of diagenetic alteration on paleotemperature reconstructions for the deep and surface ocean. We find that overall, primary Δ_{47} signatures appear similarly sensitive to diagenetic overprinting as $\delta^{18}O$, with differences in sensitivity depending on pore fluid chemistry and the amount of secondary calcite. Where planktic foraminifera are significantly altered, sea surface temperatures derived from Δ_{47} and $\delta^{18}O$ values are biased towards cool temperatures. In comparison, Δ_{47} and $\delta^{18}O$ values of benthic and well preserved planktic foraminifera are less affected by diagenesis and thus likely to yield robust foraminiferal calcification temperatures. With independent estimates of diagenetic calcite fractions, secondary overprints could be corrected for, using end-member modeling and Δ_{47}-based temperatures from benthic foraminifera.
© 2019 The Authors. Published by Elsevier Ltd. This is an open access article under the CC BY license (http://creativecommons.org/licenses/by/4.0/).

Keywords: Clumped isotopes; Foraminifera; Preservation; Diagenesis; Eocene; Stable-isotope geochemistry

1. INTRODUCTION

For decades, the geochemical composition of foraminiferal tests buried in ocean sediments has been used to reconstruct paleoceanographic conditions, addressing a large range of questions regarding forcing and response mechanisms in the climate system (e.g., Zachos et al., 2001).

* Corresponding author.
E-mail address: Thomas.Leutert@uib.no (T.J. Leutert).

The carbonate clumped isotope (Δ_{47}) paleothermometer based on the ordering of two heavy isotopes (^{13}C and ^{18}O) in the carbonate lattice (Ghosh et al., 2006; Schauble et al., 2006) is increasingly being applied in paleoceanographic research (e.g., Rodríguez-Sanz et al., 2017; Evans et al., 2018; Henkes et al., 2018). Recent advances in the analytical technique, especially in reducing sample size requirements, have greatly improved the applicability of this thermometer to foraminiferal carbonates (e.g., Meckler et al., 2014; Müller et al., 2017). Unlike other foraminifera-based proxies (e.g., Mg/Ca, $\delta^{18}O$), the clumped isotope paleothermometer is independent of the chemical composition of the parent-water body, rendering it especially suitable for applications in deep time where secular changes in seawater composition occurred. In addition, foraminiferal species-specific vital effects seem to be negligible (Tripati et al., 2010; Grauel et al., 2013; Breitenbach et al., 2018; Peral et al., 2018; Piasecki et al., 2019).

However, the reconstruction of ocean temperatures from foraminiferal carbonates requires the preservation of primary Δ_{47} signatures established during initial biogenic calcite precipitation. Post-depositional diagenesis may alter primary geochemical compositions of carbonates buried in ocean sediments, and thus bias any derived paleoclimate signal (e.g., Killingley, 1983; Delaney, 1989; Schrag, 1999; Pearson et al., 2001; Rudnicki et al., 2001; Tripati et al., 2003; Sexton et al., 2006b; Sexton and Wilson, 2009; Kozdon et al., 2011; Kozdon et al., 2013; Edgar et al., 2015; Golreihan et al., 2018). Reconstructing tropical sea surface conditions has proven to be especially challenging. $\delta^{18}O$-based sea surface temperature (SST) reconstructions for the tropics in the Cretaceous and Paleogene greenhouse climates (with atmospheric CO_2 levels several times of the preindustrial level) were found to be substantially lower than expected from model simulations, and even often cooler than tropical SSTs today (e.g., Zachos et al., 1994). This "cool tropics paradox" (Dhondt and Arthur, 1996) became an impediment to understanding greenhouse climates for several decades (Crowley and Zachos, 1999). A solution to the discrepancies between model and proxy data was proposed when the validity of much of the data (mostly $\delta^{18}O$-based SST estimates) began to be called into question (Wilson and Opdyke, 1996; Pearson et al., 2001; Sexton et al., 2006b). It was hypothesized that planktic foraminiferal calcites from the pelagic carbonate-rich drill sites normally targeted for paleoceanographic studies were compromised by diagenesis in the cold seafloor environment. It is now understood that diagenetic precipitation of secondary inorganic calcite (Pearson et al., 2001) and/or recrystallization of primary biogenic calcite (Sexton et al., 2006b) at the seafloor can lead to planktic foraminifera with artificially high $\delta^{18}O$ values and thus unrealistically low calculated paleotemperatures. Although it is often assumed that benthic foraminiferal isotopic compositions are less impacted by these diagenetic processes (Edgar et al., 2013; Voigt et al., 2016), $\delta^{18}O$ values of benthic foraminiferal tests have been shown to be susceptible to diagenetic alteration, with the extent of alteration dependent upon sediment lithology and sedimentation rate (Sexton and Wilson, 2009). Diagenetic effects also remain

problematic for most other foraminifer-based geochemical paleoproxies including Δ_{47} (e.g., Sexton et al., 2006b; Kozdon et al., 2013; Edgar et al., 2015; Stolper et al., 2018). A recent study by Stolper et al. (2018) showed that primary Δ_{47}-based SSTs measured on different size fractions of marine bulk carbonate sediments are biased towards sub-seafloor temperatures in a carbonate-rich pelagic setting, likely reflecting recrystallization and cementation in pore fluids under a geothermal gradient. To date, however, little is known about specifically how foraminiferal Δ_{47} signatures respond to diagenetic alteration on million-year timescales.

This study assesses the effects of diagenetic alteration on the foraminiferal Δ_{47} paleothermometer, using stable isotope data and Scanning Electron Microscope (SEM) imaging of middle Eocene foraminifera from multiple regions in the Atlantic Ocean. We apply the clumped isotope technique to planktic and benthic foraminifera from sediments retrieved from sites at a range of burial depths, sediment lithologies, and pore fluid chemistries, and compare the clumped isotope results with $\delta^{18}O$ data acquired from the same samples. We have two main goals with this work. First, we aim to test the reliability of Δ_{47}-based deep-sea temperature (DST) reconstructions. For that, we assume that bottom water conditions during biogenic calcite precipitation were similar at sites from similar water depths, and inter-site differences in benthic foraminiferal Δ_{47} values are attributable to diagenetic alteration. Second, we analyse planktic foraminifera from sites with contrasting sediment lithologies and burial histories to assess how resistant Δ_{47}-derived SSTs are to diagenetic alteration. The sensitivity of benthic and planktic foraminiferal paleotemperatures to diagenesis is further examined using end-member mixing modeling. Thereby, we assume varying amounts of diagenetic calcite. Finally, we compare the middle Eocene paleotemperature values of this study to existing data, exploring the possible impacts of diagenesis on reconstructions of latitudinal temperature gradients.

2. BACKGROUND: DIAGENESIS OF FORAMINIFERAL CALCITE

Post-depositional alteration of foraminiferal tests is complex and comprises several inter-related processes, which may potentially affect foraminiferal Δ_{47} signatures. The relevant processes include neomorphism, cementation, dissolution, and solid-state reordering. Neomorphism or recrystallization involves the replacement of primary biogenic calcite with larger inorganic calcite crystals (e.g., Killingley, 1983; Sexton et al., 2006b). Ultimately, the replacement of small biogenic microgranules with larger calcite crystals changes the reflective properties of a foraminiferal test (Pearson and Burgess, 2008). Non-recrystallized pristine tests without structural alteration or overgrowths tend to have a translucent ("glassy") appearance under the binocular microscope, whereas recrystallized tests appear opaque ("frosty") (Sexton et al., 2006b). However, surface microstructures such as pores and spines can be preserved even in the case of significant recrystallization. This makes it difficult to precisely assess neomorphic changes

under the light microscope. Instead, alternative analytical methods such as SEM imagery must be used for diagnosis (e.g., Sexton et al., 2006b). Cementation occurs when carbonate mineral overgrowths form on or within tests during burial. Like recrystallization, this process impacts the bulk chemistry of foraminiferal tests. Whole-test chemistry can also be affected in the water column and in sediments through partial dissolution in undersaturated waters (Brown and Elderfield, 1996). Finally, a series of studies have shown that the geochemical composition of fossils may also be altered without visually perceptible changes, for example through solid state diffusion of isotopes at high burial temperatures (Passey and Henkes, 2012; Henkes et al., 2014; Shenton et al., 2015).

The impact of most of these diagenetic processes on foraminiferal carbonate chemistry is largely controlled by factors that influence sediment-pore fluid exchange during early burial. This exchange can be intensified by low sedimentation rates and/or an overlying hiatus resulting in increased diagenetic alteration (Rudnicki et al., 2001; Sexton and Wilson, 2009). In contrast, fine clay and silt may "entomb" foraminifera limiting the interaction of their calcite with the surrounding pore fluids. It has been suggested that preservation is thus favoured by hemipelagic clay-rich lithologies and low porosities (e.g., Sexton et al., 2006b; Sexton and Wilson, 2009).

3. MATERIAL AND METHODS

3.1. Site selection

Clumped isotope data are presented from an interval spanning 500 kyr centered at magnetochron boundary 20n/20r at 43.432 Ma (Ogg, 2012; Vandenberghe et al., 2012). This time interval within the middle Eocene is characterized by a comparatively stable global climatic regime without major climate transitions or hyperthermal events (e.g., Sexton et al., 2006a; Zachos et al., 2008). 50–72 samples were taken at each study site for a temporal resolution of around 10 kyr.

We examined samples from six pelagic sites spanning a range of latitudes (Fig. 1). IODP Sites 1408 (41°26′N, 49°47′W), 1409 (41°18′N, 49°14′W) and 1410 (41°20′N, 49°10′W) were drilled on the Southeast Newfoundland Ridge (Fig. 1) representing the northernmost location of this study (Norris et al., 2014a, b, c). ODP Site 1050 (30°06′N, 76°14′W) is located on Blake Nose in the western North Atlantic (Norris et al., 1998), whereas ODP Site 1260 (09°16′N, 54°33′W) was drilled on Demerara Rise in the western equatorial Atlantic Ocean (Erbacher et al., 2004). ODP Site 1263 (28°32′S, 02°47′E) on Walvis Ridge is located in the eastern South Atlantic (Zachos et al., 2004). Table 1 summarizes the main characteristics of the sites including paleowater depth, paleolatitude and lithology. Our 500 kyr target interval at Sites 1409 and 1050 is carbonate ooze at shallow burial depths and at Sites 1408, 1410 and 1263 is at greater burial depths, whereas Site 1260 is our only site that was sampled below the ooze-chalk transition.

We investigate the effect of diagenesis on the isotopic composition of benthic foraminiferal tests by comparing
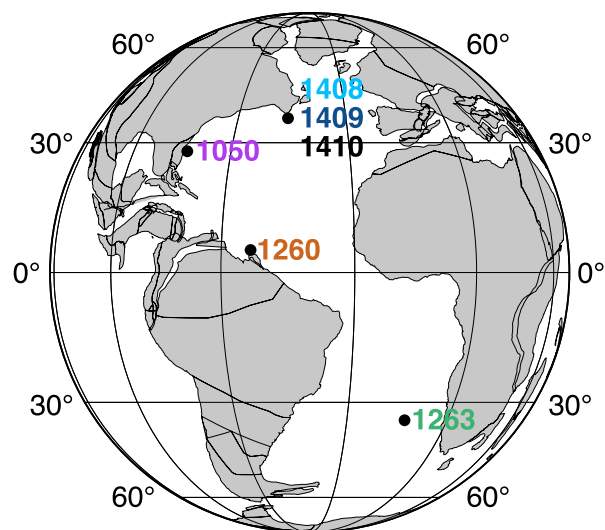

Fig. 1. Paleogeographic reconstruction of the Atlantic Ocean basin for the middle Eocene (45 Ma) showing the locations of the study sites. The base map is from the plate tectonic reconstruction service of the Ocean Drilling Stratigraphic Network (http://www.odsn.de).

results from Sites 1409, 1260 and 1263 (Fig. 1). The study sites host benthic foraminifera with different burial histories (Erbacher et al., 2004; Zachos et al., 2004; Norris et al., 2014b) but were all located in water depths between 2000 and 3000 m during the middle Eocene (Table 1). Modern bottom water temperatures are similar at each of the sites (around 2.5 to 3 °C, Fig. S1). Previous studies (e.g., Sexton et al., 2006a) suggest a relatively homogeneous Atlantic Ocean with respect to benthic foraminiferal $\delta^{18}O$ values in the time interval of this study, indicating minimal differences in DST and deep-sea water $\delta^{18}O$ values between our target sites.

Planktic foraminifera were analysed from Sites 1408, 1409, 1410, 1050, 1260 and 1263, covering a wide range of latitudes (Table 1) and preservation states, as indicated by new and previous SEM work as well as cruise report data (Norris et al., 1998; Erbacher et al., 2004; Zachos et al., 2004; Sexton et al., 2006a; Norris et al., 2014a, b, c). Sites 1050, 1260 and 1263 represent "typical" carbonate-rich pelagic ODP/IODP drill sites hosting frosty foraminifera in our target interval. Measured pore fluid Sr^{2+} profiles for Sites 1050, 1260 and 1263 are shown in Fig. S2, but not further discussed due to their limited informative value in terms of foraminiferal preservation. The foraminifera buried in the clay-rich drift sediments offshore Newfoundland at Sites 1408, 1409 and 1410 (Boyle et al., 2017) appear exceptionally well preserved. Notably, preservation may be slightly better at Sites 1408 and 1410 in comparison to Site 1409, owing to their higher sedimentation rates (e.g., Sexton and Wilson, 2009).

The benthic species used in this study was the shallow infaunal species *Nuttalides truempyi*. For planktic foraminifera, we used *Morozovelloides coronatus* (junior synonym *M. spinulosa*) at the low latitude sites (Sites 1050 and 1260) and *Acarinina bullbrooki* at the high latitude sites

Table 1
Characteristics of the study sites.

Site	Modern water depth[a] (m)	Paleowater depth[b] (m)	Paleolatitude[c]	Splice depth[d] (m)	Lithology	Porosity[a] (vol%)	Mean sedimentation rate (cm/kyr)	CaCO$_3$[a] (wt%)
1408	~3020	~2580	29.1–34.8°N	154.51–166.21	Nannofossil clay and ooze	~60	2.95	~40–50
1409	~3500	~3050	28.9–34.6°N	56.90–66.21	Nannofossil clay and ooze	~70	2.42	~40–50
1410	~3390	~2950	28.9–34.6°N	159.25–170.28	Nannofossil clay and ooze	~60	3.07	~40–50
1050	~2300	~1000–2000	21.7–27.4°N	57.04–72.84	Nannofossil ooze	~60	3.31	~70
1260	~2550	~2500–3200	2.5°S–3.2°N	117.21–128.88	Radiolarian and nannofossil chalk	~60–70	2.34	~70–80
1263	~2720	~2000–3000	37.1–42.8°S	169.82–174.22	Nannofossil ooze	~50	0.88	~90

[a] Shipboard measurements (Norris et al., 1998; Erbacher et al., 2004; Zachos et al., 2004; Norris et al., 2014a, b, c).
[b] From Tucholke and Vogt, 1979 (Sites 1408, 1409, 1410; around 50 Ma), Norris et al., 1998 (Site 1050), Sexton et al., 2006a (Site 1260) and Zachos et al., 2004 (Site 1263).
[c] Calculated using the paleolatitude calculator (http://www.paleolatitude.org) of van Hinsbergen et al. (2015) with the paleomagnetic reference frame from Torsvik et al. (2012).
[d] We use the shipboard composite depth scale for Site 1050 (Norris et al., 1998). The composite depth scales of Sites 1408 and 1410 used in this study are published in Boulila et al. (2018), whereas the revised shipboard composite depth scales of Sites 1409, 1260 and 1263 are from Hull et al. (2017), Westerhold and Röhl (2013) and Westerhold et al. (2015), respectively.

(Sites 1408, 1409, 1410 and 1263). Both species are thought to have been upper ocean mixed-layer dwellers (Pearson et al., 2006; Sexton et al., 2006c).

3.2. Age models

All ages are given in Myr relative to magnetochron boundary 20n/20r. This boundary is well documented in the magnetostratigraphies (e.g., inclination data) of all sites and serves as our primary age tie point (Ogg and Bardot, 2001; Erbacher et al., 2004; Edgar et al., 2007; Norris et al., 2014a, b, c; Westerhold et al., 2015). Age models for Sites 1408, 1410, 1260 and 1263 have been astronomically calibrated using XRF time series (Westerhold and Röhl, 2013; Westerhold et al., 2015; Hull et al., 2017; Boulila et al., 2018). However, the calibrated age model of Site 1260 was based on an older astronomical solution (Laskar et al., 2004; Westerhold and Röhl, 2013) in comparison to those of Sites 1408, 1410 and 1263 (Laskar et al., 2011a; Laskar et al., 2011b; Westerhold et al., 2015; Boulila et al., 2018). Therefore, we updated Site 1260′s age model by tuning its benthic $\delta^{13}C$ record to that from Site 1263 which shows excellent correlation with the La2010d eccentricity (Laskar et al., 2011a), resulting in a forward shift of absolute ages (younging) by 40 kyr (Fig. S3). Tuning benthic $\delta^{13}C$ at these two sites is considered reasonable because the pronounced cyclicities of (bulk and benthic) $\delta^{13}C$ in middle Eocene sequences have been observed to consistently covary with eccentricity and have thus been used for orbital tuning (e.g., Westerhold et al., 2015). The age model for Site 1409 was built in two steps: First, an age model was established based on linear interpolation between magnetostratigraphic dates (in Myr relative to 20n-20r boundary) on the GTS2012 timescale (Ogg, 2012; Vandenberghe et al., 2012). Second, Site 1409 was correlated to Site 1263, using the eccentricity cycles preserved in benthic foraminiferal $\delta^{13}C$ (Fig. S4; Table S1). At Site 1050, benthic foraminifera were not analysed, and planktic $\delta^{18}O$ and $\delta^{13}C$ values were deemed too variable for correlation. Therefore, the age model of Site 1050 was built based on the assumptions of linear sedimentation rates between the magnetochron boundaries (Ogg and Bardot, 2001) and magnetochron durations of GTS2012 (Ogg, 2012; Vandenberghe et al., 2012).

3.3. Sample preparation

Sediment samples (25 cm^3) from Sites 1409 (n = 72), 1410 (n = 50), 1050 (n = 50), 1260 (n = 50) and 1263 (n = 50) were freeze-dried and then wet-sieved through a 63 μm mesh at the University of Bergen, whereas samples from Site 1408 (30 cm^3, n = 65) were prepared for picking at Yale University (Hull et al., 2017). Planktic foraminifera were picked from a narrow size fraction from 250 μm to 355 μm. For benthic foraminifera, the range was extended (150–355 μm) to obtain enough specimens for isotope analysis.

As the goal of the study is to assess the impact of diagenesis on the application of foraminiferal Δ_{47} in paleoceanograhic research, samples were treated as commonly

done for paleoceanographic studies, mainly to remove infillings consisting of non-foraminiferal carbonate. To this end, we gently cracked specimens from each sample between two glass plates to open test chambers. After cracking, test fragments were rigorously cleaned as follows: Planktic foraminifera were ultrasonicated three times for 30 seconds in deionized water and one time for 30 seconds in methanol. The same cleaning protocol was used for benthic foraminifera but with only ten seconds of ultrasonication in methanol. Between each cleaning step, we brought test fragments into suspension, let the fragments settle and pipetted off the overlying solution which may contain potential contaminants (e.g., clay). After the last ultrasonication step, test fragments were rinsed at least three times (until the solute was clear and no longer milky) to remove any methanol and/or remaining clay particles. Before being weighed out for analysis, all samples were oven-dried at 50 °C and checked under the microscope for any remaining contaminants (e.g., black stains).

For SEM analysis, foraminiferal specimens were ultrasonicated in water for a few seconds, rinsed until the water became clear and then dried. Next, we mounted them on SEM stubs using adhesive carbon tabs. Coated with gold/palladium, they were photographed using a Zeiss Supra 55VP scanning electron microscope at the University of Bergen.

3.4. Measurement and processing of stable isotope data

The abundance of "clumped" carbonate ions containing both ^{13}C and ^{18}O isotopes is low (e.g., Ghosh et al., 2006). This low abundance leads to relatively large sample size requirements as the precision required for paleoclimate applications needs to be obtained by averaging over numerous replicate measurements (Thiagarajan et al., 2011; Meckler et al., 2014; Fernandez et al., 2017). Obtaining large sample amounts is challenging in foraminifera-based paleoceanography, where specimens of a given species are usually very limited in quantity. Yet recent advances in the analytical technique, especially in reducing sample size requirements, have greatly improved the applicability of this thermometer to foraminiferal tests (e.g., Meckler et al., 2014; Müller et al., 2017).

In this study, we use a recently developed measurement approach based on replicate measurements of very small (on the order of 100 µg) carbonate samples (e.g., Schmid and Bernasconi, 2010; Hu et al., 2014; Meckler et al., 2014). The necessary precision is achieved by pooling clumped isotope measurements of a large number of adjacent samples from a relatively stable climate interval (e.g., Grauel et al., 2013; Rodríguez-Sanz et al., 2017). We also average over a comparably large number of aliquot measurements within the time interval of interest to avoid aliasing and to maximize the overlap in time among the sites. Each clumped isotope sample value interpreted in this study is the average over 51–99 analyses of ~120 µg each (roughly 6–12 mg calcite per site and species in total). Some samples were measured more than once where foraminifera abundance allowed. In parallel with the average clumped isotope temperature for each climate interval, the method yields

higher-resolution $\delta^{18}O$ and $\delta^{13}C$ data. Sample errors (precision) of Δ_{47} values are reported as the standard error of the mean (SE). ± 1 SE and 68% confidence interval as well as ± 2 SE and 95% confidence interval are almost indistinguishable, because of the large number of analyses for each reported clumped isotope temperature (>50 measurements). Δ_{47} values are given with four decimals to avoid rounding errors in further calculations.

All isotope analyses were carried out on a Thermo Scientific MAT 253 Plus mass spectrometer coupled to a Kiel IV carbonate preparation device (described in Schmid and Bernasconi, 2010). The Kiel device has been modified with a Porapak trap to eliminate organic contaminants. Clumped isotope compositions of foraminiferal calcites were measured in micro-volume mode with the long-integration dual-inlet (LIDI) method (Hu et al., 2014). We used the software "Easotope" (John and Bowen, 2016) for data processing. Clumped isotope values were standardized and monitored with four carbonate standards (ETH 1, 2, 3 and 4) of different composition and ordering state. Three of these carbonate standards were used to calculate Δ_{47} values from the background-corrected beam signals. A fourth carbonate standard was treated as a sample and used to monitor instrument performance. In every 23 h-run, 4–5 of each of these carbonate standards were included. The external reproducibilities (1σ standard deviation) of ETH 1, 2, 3 and 4 after correction range from 0.0308‰ to 0.0385‰. All carbonate $\delta^{18}O$ and $\delta^{13}C$ values are given relative to the VPDB scale and corrected with the same carbonate standards as used for clumped isotope corrections. Water $\delta^{18}O$ values are given relative to VSMOW. For $\delta^{18}O$ and $\delta^{13}C$, the mean 1σ external reproducibilities of the standards are 0.04–0.11‰ and 0.02–0.06‰, respectively. Sample and standard data are listed in Tables S2 and S3. Table S4 contains the reproducibilities of all standards for Δ_{47}, $\delta^{18}O$ and $\delta^{13}C$. Further details on the analysis of clumped isotopes and data correction can be found in Appendix A.1.

Clumped isotope paleotemperatures were calculated from the corrected mean Δ_{47} values using the travertine-based calibration of Kele et al. (2015), which was recalculated by Bernasconi et al. (2018). The recalculated travertine (Kele) calibration is based on similar analytical and data processing methods (e.g., Kiel device, Brand parameters, acid fractionation factor, standard values) as those employed at the University of Bergen, spans a large temperature range (6–95 °C) and shows a good agreement with an in-house calibration based on foraminifera (Piasecki et al., 2019). Calibration and analytical uncertainties in clumped isotope temperatures are fully propagated (see supporting information of Huntington et al. (2009) for description of error propagation procedure).

Eq. (1) of Bemis et al. (1998) is an oxygen isotope temperature calibration providing a good fit to modern Cibicidoides spp. and mixed layer dwelling planktic foraminifera. We used this calibration to calculate mean deep-sea water $\delta^{18}O$ compositions from benthic foraminiferal $\delta^{18}O$ and clumped isotope DST values measured on the same samples at each site. For that, we corrected our Nuttalides truempyi $\delta^{18}O$ data to Cibicidoides spp. with the correction factor for

δ^{18}O ((Nut + 0.10)/0.89) from Katz et al. (2003). The calibration error of Eq. (1) of Bemis et al. (1998) is not included in our calculations, due to the dominance of other major uncertainties inherent in the application of this equation to middle Eocene foraminifera (e.g., vital effects).

We also used Eq. (1) of Bemis et al. (1998) to calculate DST values from *N. truempyi* δ^{18}O values normalized to *Cibicidoides* spp. (Katz et al., 2003) and prescribed deep-sea water δ^{18}O values. Thereby, deep-sea water δ^{18}O compositions were assumed to be identical at all sites and approximated by the previously calculated deep-sea water δ^{18}O values averaged over all sites. We acknowledge some degree of circularity in these DST calculations based on benthic foraminiferal δ^{18}O and deep-sea water δ^{18}O values, leading to δ^{18}O-based DSTs that are very similar to our Δ_{47} DSTs. However, due to the averaging of our deep-sea water δ^{18}O values across all sites, potential relative differences in DST between the sites should be preserved, allowing us to assess the effects of diagenesis on δ^{18}O-based DST values.

Furthermore, we used the average of our deep-sea water δ^{18}O values as a basis to calculate surface water δ^{18}O values at each site following Eq. (1) of Zachos et al. (1994) to correct for latitudinal variation in surface δ^{18}O, with the caveat that surface water δ^{18}O distributions during the Eocene are highly uncertain. Then, we calculated SSTs from surface water δ^{18}O and planktic foraminiferal δ^{18}O values again with Eq. (1) of Bemis et al. (1998).

3.5. Modeling the effect of diagenesis

Similar to previous studies (e.g., Pearson et al., 2001; Tripati et al., 2003), we use the concept of a two component mixing line between a primary and secondary end-member to explore the effects of diagenesis on the isotopic composition of benthic and planktic foraminiferal tests, and hence their usefulness as a paleothermometer. This simple approach, based on the assumption of inorganic calcite precipitating in exchange with pore fluids ("open" system), is extended from the carbon and oxygen isotope systems to the clumped isotope system, and applied at Sites 1260 and 1263. At these carbonate-rich sites, foraminiferal tests show clear signs of diagenetic alteration, in contrast to the well-preserved foraminifera buried in the clay-rich sediments at Site 1409. Furthermore, isotope data measured on benthic foraminifera from Site 1260 as well as Site 1263 provide a basis to approximate the site-specific isotopic composition of secondary inorganic calcite (described in next paragraph). The calculated diagenetic trajectories across different preservation states provide constraints on the sensitivity of δ^{18}O- and Δ_{47}-based paleotemperature estimates to diagenetic alteration, but do not factor in potential impacts purely from dissolution or the possibility of multiple or time-variant end-members.

The model assumes that diagenetic alteration occurs in the uppermost pore fluids, in keeping with other recent work (e.g., Rudnicki et al., 2001; Edgar et al., 2013; Voigt et al., 2016). Pore fluid δ^{18}O of the precipitating phase is estimated from benthic foraminiferal δ^{18}O (*N. truempyi* values normalized to *Cibicidoides* spp.) utilizing the calibration of Bemis et al. (1998) with site-specific benthic clumped isotope temperatures (Table 2). Then, pore fluid δ^{18}O is used to calculate inorganic calcite δ^{18}O values. For that, we follow two different temperature-dependent abiogenic calcite-water oxygen isotope fractionation relationships, determined by Watkins et al. (2013) and Kim and O'Neil (1997). The fractionation factor ($\alpha_{c\text{-}w}$) of Watkins et al. (2013) describes ^{18}O fractionation between water and carbonate corresponding to slow, equilibrium growth of inorganic calcite (Fantle and DePaolo, 2007). In contrast to Watkins et al. (2013), Kim and O'Neil (1997) derived their equilibrium curve from calcites that were grown at rates too high for equilibrium (Watkins et al., 2014). The fractionation factor of Kim and O'Neil (1997) thus describes non-equilibrium growth of calcite at higher growth rates in comparison to the fractionation factor of Watkins et al. (2013). Similar to previous studies on diagenesis (e.g., Schrag, 1999; Stolper et al., 2018), effects on $\alpha_{c\text{-}w}$ other than temperature (e.g., pH) are ignored for simplicity and owing to lack of constraints.

The inferred δ^{13}C signature of inorganic calcite precipitated in pelagic sediments with high carbonate but low organic matter content tends to be similar to bulk carbonate δ^{13}C values (e.g., Edgar et al., 2015; Voigt et al., 2016). Therefore, we approximate inorganic calcite δ^{13}C by bulk δ^{13}C values in our model (Table 2). We did not measure bulk δ^{13}C in this study. Bulk δ^{13}C data for Site 1263 were taken from Westerhold et al. (2015) and averaged over the study interval. For Site 1260, bulk δ^{13}C data were not available for the exact interval of this study. Therefore, bulk δ^{13}C values from Edgar et al. (2007) were averaged over a slightly younger interval (41.856 to 41.871 Ma, 75.485–75.785 m composite depth at their scale) before the Middle Eocene Climate Optimum, assuming values similar to the interval of this study. In addition, we tested our model using δ^{13}C values that are higher and lower than bulk δ^{13}C as well as our planktic δ^{13}C values to approximate inorganic δ^{13}C. The latter approach has been previously applied by Edgar et al. (2015).

A major source of uncertainty for our model, as for previous modeling work, in correcting paleotemperature estimates for diagenetic effects is the amount of secondary inorganic calcite present in a frosty (*sensu* Sexton et al., 2006b) foraminiferal test (e.g., Tripati et al., 2003). Conventional SEM imagery does not allow for a quantitative assessment of diagenetic alteration. Indirect estimates for typical pelagic settings range widely, from around 15% to more than 50% secondary calcite (Pearson et al., 2001; Tripati et al., 2003; Kozdon et al., 2011; Edgar et al., 2015). Characterisation techniques such as electron backscatter diffraction (EBSD) have recently opened the possibility of more quantitatively estimating the fraction of diagenetic calcite in foraminiferal tests, and are currently being explored elsewhere (Tripati et al., 2017). With this future prospect in mind, we assess the sensitivity of our paleothermometers to various degrees of overprinting. We solve mass balance equations with diagenetic end-member contributions of 10, 20, 30, 40 and 50%. For δ^{18}O, we assume linear mixing:

$$\delta^{18}O_{frosty} = F_{diag} \times \delta^{18}O_{diag} + (1 - F_{diag}) \times \delta^{18}O_{glassy} \quad (1)$$

Table 2
Hypothesized composition of inorganic calcite formed during early diagenesis. Inorganic calcite compositions used for our deep-sea temperature (DST) and sea surface temperature (SST) modeling are slightly different, because the overlapping time interval (and thus also the corresponding averaging interval) of our benthic isotope records is around 20 kyr longer than the overlapping interval of our planktic records (Figs. 4 and 5).

Site	Bottom water temperature[a] (°C)	Pore fluid $\delta^{18}O$[b] (‰)	α_{c-w} Watkins et al. (2013)[c]	α_{c-w} Kim and O'Neil (1997)	Inorg. calcite $\delta^{18}O$ Watkins et al. (2013) (‰)	Inorg. calcite $\delta^{18}O$ Kim and O'Neil (1997) (‰)	Inorg. calcite $\delta^{13}C$[d] (‰)	Inorg. calcite Δ_{47}[e] (‰)
Modeling of DSTs								
1260	12.6	−0.20	1.03285	1.03114	1.67	0.01	1.19	0.7167
1263	12.2	−0.17	1.03295	1.03124	1.80	0.14	2.02	0.7184
Modeling of SSTs								
1260	12.9	−0.15	1.03279	1.03108	1.65	0.00	1.19	0.7156
1263	12.5	−0.11	1.03288	1.03118	1.79	0.14	2.02	0.7173

[a] From the Δ_{47} signatures of benthic foraminifera averaged over relevant time interval.
[b] Derived from benthic foraminiferal $\delta^{18}O$ averaged over relevant time interval using Eq. (1) of Bemis et al. (1998).
[c] Based on α_{c-w} of Watkins et al. (2013), as shown in Eq. (19) of Watkins et al. (2014).
[d] Derived from bulk $\delta^{13}C$ (Edgar et al., 2007; Westerhold et al., 2015), as described in material and methods.
[e] Benthic foraminiferal Δ_{47} averaged over relevant interval.

F_{diag} is the fraction of the diagenetic end-member. Subscript text refers to the isotopic composition of measured frosty foraminiferal calcite (frosty), pristine glassy foraminiferal calcite (glassy) and inorganic diagenetic calcite (diag). Eq. (1) is then solved for $\delta^{18}O_{glassy}$ in order to estimate glassy foraminiferal $\delta^{18}O$ values. Similar calculations are carried out for $\delta^{13}C$.

In contrast to $\delta^{18}O$ and $\delta^{13}C$, Δ_{47} mixing is non-linear depending on the Δ_{47}, $\delta^{18}O$ and $\delta^{13}C$ values of the end-members (e.g., Eiler and Schauble, 2004; Defliese and Lohmann, 2015). We adopt the non-linear mixing model described in Defliese and Lohmann (2015) to calculate glassy foraminiferal Δ_{47} values from frosty foraminiferal Δ_{47} for different fractions of diagenetic calcite (see Appendix A.2 for further details). In order to test the sensitivity of the calculations to the type of mixing model, we additionally performed linear mixing calculations.

4. RESULTS

4.1. Foraminiferal preservation

Under the light microscope, benthic foraminifera from Site 1409 appear exceptionally well preserved (mostly translucent and glassy), whereas benthic foraminifera from Sites 1260 and 1263 are characterized by noticeably poorer (frosty) states of preservation (see Fig. S5 for preservation ranges of the benthic foraminiferal tests). This impression is confirmed by SEM analysis, which reveals much smoother surface textures of benthic foraminiferal tests at Site 1409 in comparison to Sites 1260 and 1263 (Fig. 2). Benthic foraminifera from Sites 1260 and 1263 are characterized by overgrowths of coarse inorganic crystallites with clearly visible crystal faces covering both surface and interior test walls (examples indicated by white arrows in Fig. 2e and g). The wall cross sections of *N. truempyi* from Site 1409 show calcite that is somewhat denser and more microgranular than at Sites 1260 and 1263 (Fig. 2g, h and i). However, benthic foraminiferal calcites from Sites 1260 and 1263 do not appear pervasively recrystallized. Additional SEM images documenting benthic foraminiferal preservation at each study site are shown in Fig. S6.

Planktic foraminifera from Sites 1050, 1260 and 1263 exhibit "blocky" textures and clear crystal faces (e.g., Pearson and Burgess, 2008), consistent with post-depositional alteration (Fig. 3). Crystallographic planes are most pronounced at Site 1263 and slightly less so at Site 1260, where fine wall structures such as tubular pore channels are visible in the wall cross section (Fig. 3h). Specimens from Site 1050 appear less granular in wall texture than those at Sites 1260 and 1263. Tests of *A. bullbrooki* examined at Sites 1408, 1409 and 1410 do not have large blocky crystals and do exhibit a number of fine wall structures, consistent with better calcite preservation. Some specimens show slightly uneven surfaces, covered by a thin layer of sub-micron crystals (Fig. 3m and n). These may be diagenetic in origin (cemented overgrowths) or could be part of the internal microstructure, exposed through minor partial dissolution (e.g., Pearson and Burgess, 2008). In contrast to the sites hosting frosty foraminifera, the Primary Organic
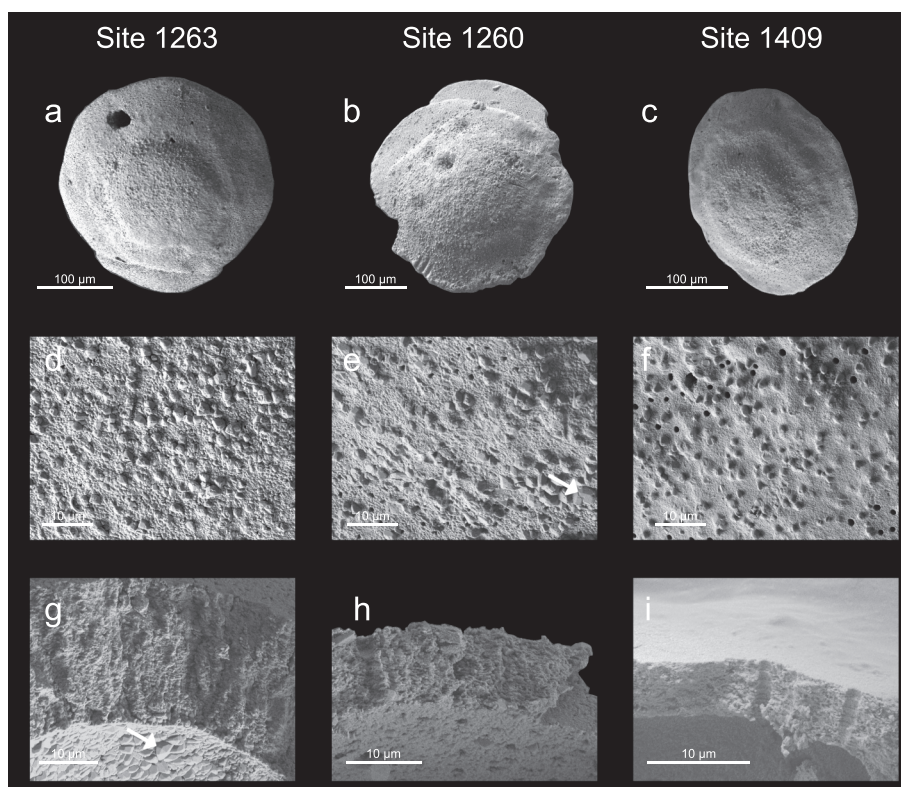
Fig. 2. SEM images showing the preservation state of benthic foraminifera *N. truempyi* at Sites 1263 (a, d, g), 1260 (b, e, h) and 1409 (c, f, i). Whole test images (a-c) do not reveal large differences in appearance, but when viewed in detail (d-i), the better preservation of the glassy benthic foraminiferal tests from Site 1409 is apparent. Scale bars are 100 μm (a-c) and 10 μm (d-i). The foraminifera were picked from samples 208-1263B-11H-4,91–93 (a, d, g), 207-1260B-10R-6,94–96 (b, e, h) and 342-U1409C-7H-4,110–112 (c, f, i). See Fig. S6 for additional images.

Membrane (POM) is clearly visible in the wall cross sections of the specimens from Sites 1408, 1409 and 1410 offshore Newfoundland (indicated by white arrows in Fig. 3p, q and r). Furthermore, many planktic foraminifera from these sites show substantial infillings (e.g., clay) in the aperture (Fig. 3k). However, our extensive cleaning protocol is designed to completely remove clay infillings before isotope analysis. In general, the foraminifera at Sites 1408, 1409 and 1410 exhibit broadly similar ranges of preservation (see Fig. S7 for preservation ranges of the planktic foraminiferal tests), despite their different sub-seafloor burial depths. This highlights the crucial role played by lithology (in this case, clay-rich sediments) in enhancing microfossil preservation (e.g., Sexton et al., 2006b; Sexton and Wilson, 2009). SEM images of further representative planktic foraminiferal specimens for each study site can be found in Figs. S8 and S9.

4.2. Foraminiferal $\delta^{18}O$, $\delta^{13}C$ and Δ_{47} values

Our high-resolution ($\sim$10 kyr) middle Eocene isotope records were used to define overlapping intervals for all benthic and planktic foraminiferal records (Figs. 4 and 5). The benthic isotope records overlap from approximately -0.17 Myr to $+0.21$ Myr around the 20n/20r boundary (marked by horizontal bar in Fig. 4), whereas the planktic records, which comprise more sites, overlap from approximately -0.15 Myr to $+0.21$ Myr (marked by horizontal

bar in Fig. 5). To allow direct comparison, we only interpret averaged Δ_{47}- and $\delta^{18}O$-based temperature data from the abovementioned overlapping intervals.

Benthic $\delta^{18}O$ and $\delta^{13}C$ show synchronous low-frequency fluctuations (Fig. 4) following eccentricity cycles, especially pronounced from -0.1 Myr to $+0.2$ Myr at all sites. At times of high eccentricity (e.g., around $+0.1$ Myr), $\delta^{18}O$ values decrease, with an overall amplitude of roughly 0.2–0.3‰ (Fig. 4b). Using the equation of Bemis et al. (1998) and assuming no changes in global ice volume, these declines in $\delta^{18}O$ correspond to modest DST changes of approximately 1.0–1.5 °C. We observe slight offsets in mean benthic $\delta^{18}O$ ($+0.1$‰ to $+0.3$‰) and $\delta^{13}C$ ($+0.2$‰ to $+0.4$‰) values of Site 1263 in the South Atlantic relative to the more northern sites (Fig. 4b, c, S10a and S11a). As expected, the Δ_{47} signal appears very noisy in comparison to $\delta^{13}C$ and $\delta^{18}O$ (Fig. 4). Due to the large analytical uncertainty when measuring small samples, single measurements of Δ_{47} cannot be taken at face value. Average benthic foraminiferal Δ_{47} values for the overlapping time interval are 0.7145 ± 0.0028‰ (1SE) at Site 1409, 0.7167 ± 0.0042‰ at Site 1260 and 0.7184 ± 0.0045‰ at Site 1263.

Orbital-scale cyclicity appears less pronounced in the planktic $\delta^{18}O$ and $\delta^{13}C$ time series (Fig. 5) in comparison to benthic $\delta^{18}O$ and $\delta^{13}C$ (Fig. 4). Based on visual assessment, planktic $\delta^{13}C$ fluctuations are synchronous with eccentricity to a certain extent, especially at Sites 1410, 1260 and 1263, whereas changes in $\delta^{18}O$ are small (mostly < 0.5‰).
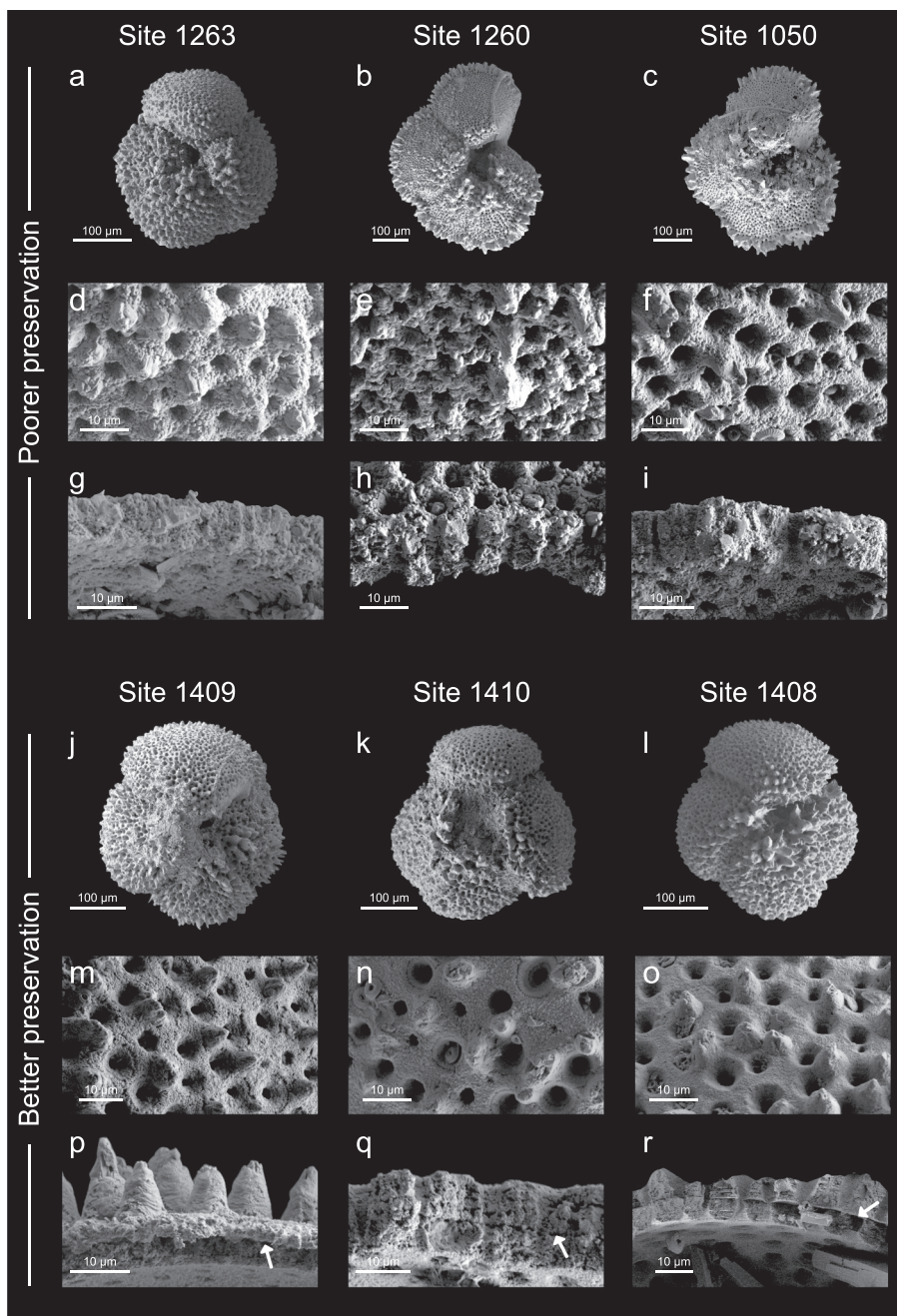
Fig. 3. SEM images showing planktic foraminiferal specimens of *M. coronatus* and *A. bullbrooki* representing the preservation states at Sites 1263 (a, d, g), 1260 (b, e, h). 1050 (c, f, i), 1409 (j, m, p), 1410 (k, n, q) and 1408 (l, o, r). Scale bars are 100 μm (a-c, j-l) and 10 μm (d-i, m-r). The foraminifera were picked from samples 208-1263B-11H-6,51–53 (a, d, g), 207-1260A-14R-5,146–148 (b, e, h), 171B-1050A-7H-5,102–104 (c, f, i), 342-U1409C-7H-2,136–138 (j, m, p), 342-U1410C-17X-4,46–48 (k, n), 342-U1410C-17X-3,73–75 (q), 342-U1408C-17H-3,37–39 (l, o) and 342-U1408B-18H-2,109–111 (r). See Figs. S8 and S9 for additional images.

Planktic foraminiferal Δ_{47} values averaged over the overlapping time interval are 0.6732 ± 0.0048 (1SE)‰ at Site 1408, 0.6767 ± 0.0044‰ at Site 1409, 0.6674 ± 0.0039‰ at Site 1410, 0.6677 ± 0.0047‰ at Site 1050, 0.6698 ± 0.0037‰ at Site 1260 and 0.6914 ± 0.0032‰ at Site 1263. Boxplots for benthic and planktic $\delta^{13}C$, $\delta^{18}O$ and Δ_{47} values at each site are shown in Figs. S10, S11 and S12.

4.3. Reconstructed deep-sea temperature and water $\delta^{18}O$ values

Benthic foraminiferal clumped isotope DSTs averaged over the studied interval (marked by horizontal bar in Fig. 4) amount to 13.2 ± 0.9 (1SE) °C at Site 1409, 12.6 ± 1.2 °C at Site 1260 and 12.2 ± 1.3 °C at Site 1263
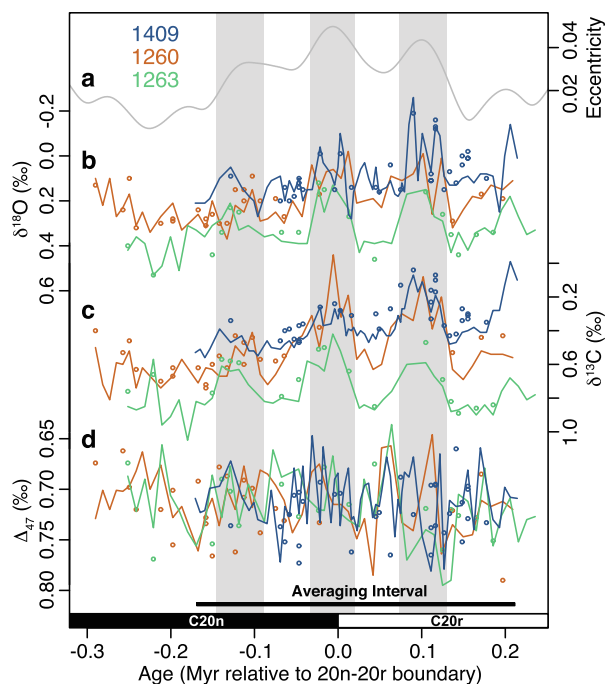
Fig. 4. Benthic $\delta^{18}O$ (b) and $\delta^{13}C$ (c) records of Sites 1409, 1260 and 1263 plotted with Δ_{47} (d) and eccentricity (a) of orbital solution La2010d (Laskar et al., 2011a). Lines are based on one measurement at each depth. Additional replicate measurements on some samples are shown as open circles and eccentricity maxima are highlighted with gray shading.

(Fig. 6a). By combining mean clumped isotope temperature data with mean benthic $\delta^{18}O$, we estimate deep-sea water $\delta^{18}O$ compositions. Average deep-sea water $\delta^{18}O$ values at Sites 1409, 1260 and 1263 are -0.20 ± 0.19 (1SE)‰, -0.20 ± 0.26‰, and -0.17 ± 0.27‰, respectively (Fig. 6b). Our deep-sea water $\delta^{18}O$ values are in good agreement with each other, but are higher than the values from a global composite of reconstructed water $\delta^{18}O$ of approximately -0.60‰ (mean during study interval), based on combining benthic foraminiferal Mg/Ca and $\delta^{18}O$ values (Cramer et al., 2011). Using the average of our calculated $\delta^{18}O$ seawater values across the three sites (-0.19‰), DST values calculated from benthic $\delta^{18}O$ for each site, averaged over the studied interval, are 13.3 °C for Site 1409, 12.7 °C for Site 1260 and 12.1 °C for Site 1263 with absolute ranges of 2.9 °C, 2.1 °C and 1.8 °C, respectively (Fig. 6a).

4.4. Sea surface temperatures

Average clumped isotope SSTs are 24.7 ± 1.5 (1SE) °C, 23.6 ± 1.4 °C, 26.4 ± 1.3 °C, 26.3 ± 1.5 °C, 25.7 ± 1.2 °C and 19.5 ± 1.0 °C at Sites 1408, 1409, 1410, 1050, 1260 and 1263, respectively (Fig. 7). We also calculate $\delta^{18}O$-based SST values, acknowledging high uncertainty owing to our limited knowledge of past surface seawater $\delta^{18}O$ values. The latter are impacted by changes in the hydrological cycle, in addition to global ice-volume and temperature (e.g., Roberts et al., 2011). Here, we estimate surface water $\delta^{18}O$ values from deep water $\delta^{18}O$ (our mean Atlantic deep-sea water $\delta^{18}O = -0.19$‰), and correct for
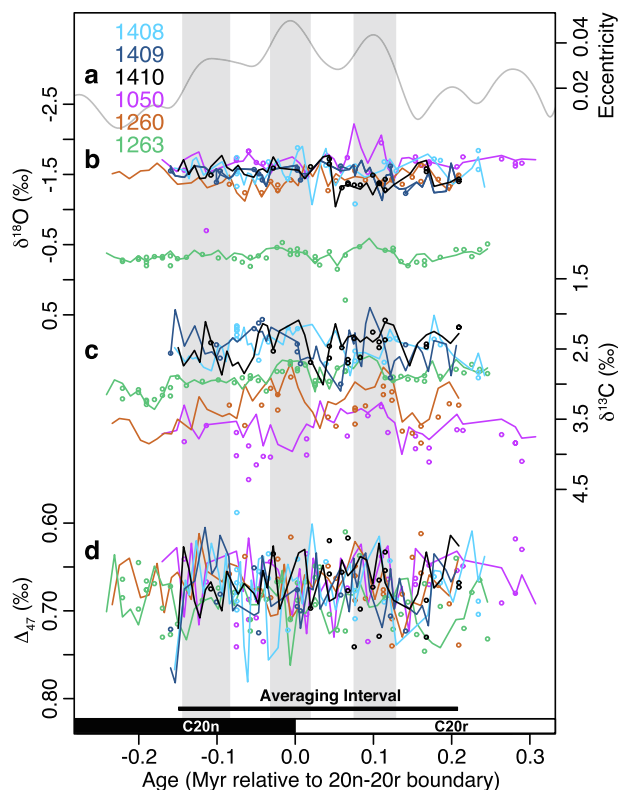

Fig. 5. (a) Eccentricity of orbital solution La2010d (Laskar et al., 2011a) as well as planktic foraminiferal (b) $\delta^{18}O$, (c) $\delta^{13}C$ and (d) Δ_{47} time series. Lines are based on one measurement at each depth. Additional replicate measurements on some samples are shown as open circles and eccentricity maxima are highlighted with gray shading.

paleolatitude (Eq. (1) of Zachos et al. (1994)), with the caveat that latitudinal gradients may have shifted. Final adjusted surface water $\delta^{18}O$ estimates are 0.82‰, 0.65‰ and 0.42‰ at Sites 1050, 1260 and 1263, respectively, and 0.65‰ at Sites 1408, 1409 and 1410. Using these surface water $\delta^{18}O$ values to calculate mean $\delta^{18}O$-based SSTs for each site with the oxygen isotope paleotemperature equation of Bemis et al. (1998), we estimate average values at Sites 1408, 1409, 1410, 1050, 1260 and 1263 of 25.9 °C, 25.5 °C, 25.5 °C, 27.2 °C, 25.1 °C and 18.9 °C, respectively (Fig. 7). Due to the large, unquantifiable uncertainties associated with our estimates for surface water $\delta^{18}O$ compositions, we do not report error estimates for surface water $\delta^{18}O$ values and the resulting SSTs. Most $\delta^{18}O$-based SST values fall within the uncertainty of the respective mean clumped isotope temperature. In comparison to $\delta^{18}O$, Δ_{47} signatures indicate slightly higher SSTs at Sites 1410, 1260 and 1263, and slightly lower SSTs at Sites 1408, 1409 and 1050.

5. DISCUSSION

5.1. Impact of diagenesis on benthic foraminiferal $\delta^{18}O$ and Δ_{47} values

Orbital-scale variations in benthic $\delta^{18}O$ and $\delta^{13}C$ time series are evident in our benthic foraminiferal records (Fig. 4). During the middle Eocene these variations should

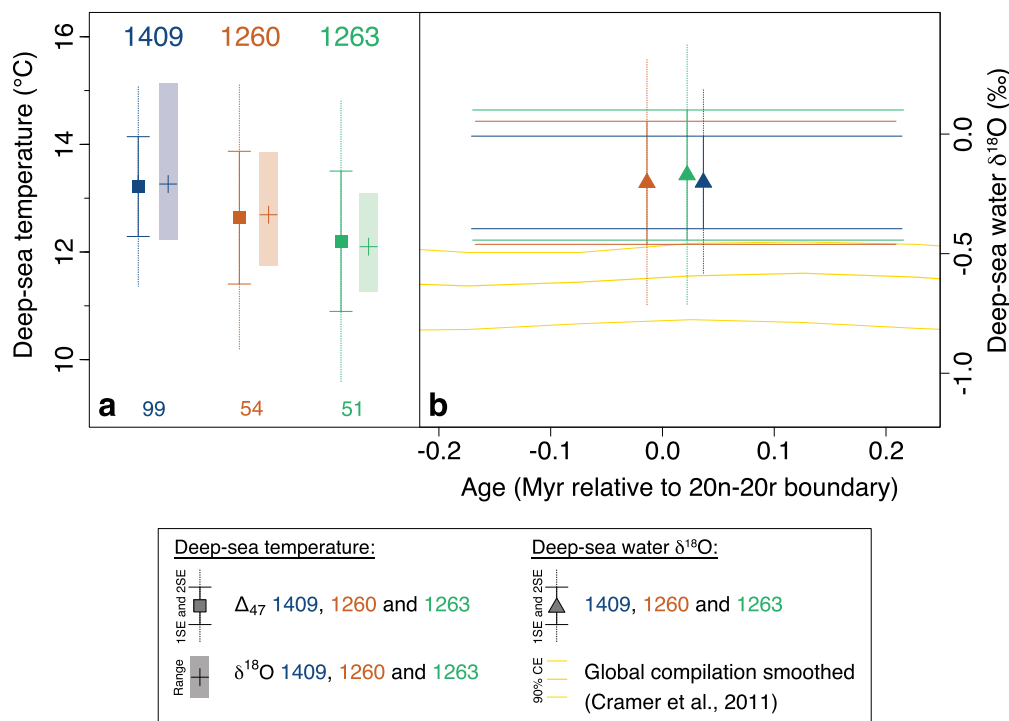Fig. 6. (a) Comparison of benthic deep-sea temperatures based on Δ_{47} (squares) and $\delta^{18}O$ (plus signs) averaged over the overlapping time interval (illustrated in Fig. 4). For Δ_{47}-based temperatures, $\pm1SE$ and $\pm2SE$ are shown using solid and dotted lines, respectively. The number of measurements used for the calculation of each temperature value are listed below. Value ranges of $\delta^{18}O$-based temperatures are illustrated with shaded bars. (b) Calculated mean deep-sea water $\delta^{18}O$ (triangles). Here, an error bar represents the propagated analytical error in Δ_{47} and $\delta^{18}O$ (solid lines = $\pm1SE$, dotted lines = $\pm2SE$) and spans exactly the respective averaging time interval, with the location of a triangle indicating its mean age. In addition, we show a global deep-sea water $\delta^{18}O$ time series based on a compilation of Mg/Ca and $\delta^{18}O$ records (Cramer et al., 2011). The dataset of Cramer et al. (2011) is plotted with their 90% confidence envelope (CE).

include eccentricity modulation of bottom water conditions (e.g., Sexton et al., 2011; Westerhold and Röhl, 2013). Such variations are observed in the benthic $\delta^{18}O$ and $\delta^{13}C$ time series at all sites, despite contrasting burial histories (Fig. 4b and c), implying that diagenetic alteration did not occur to the extent that would erase this signal. Furthermore, mean $\delta^{18}O$- and Δ_{47}-based DST values derived from glassy benthic foraminifera at Site 1409 agree well with the corresponding temperatures measured on frosty foraminifera from Sites 1260 and 1263 (Fig. 6a). The agreement in mean deep-sea water $\delta^{18}O$ values is even better (Fig. 6b). These observations suggest a negligible impact of secondary diagenetic alteration on the $\delta^{18}O$ and Δ_{47} signatures of benthic foraminiferal calcites at Sites 1409, 1260 and 1263.

We acknowledge that gradients in deep-sea water $\delta^{18}O$ and/or DST between the different sites being examined could, in theory, mask some of the potential effects of differential diagenetic processes, but we consider this possibility as less likely. Our deep-sea water $\delta^{18}O$ values are higher in comparison to the values from the global composite record of Cramer et al. (2011), based on Mg/Ca. This difference could be due to water mass differences between the ocean basins, and/or additional effects on Mg/Ca such as carbonate ion concentration (e.g., Lear et al., 2010) or a varying Mg/Ca ratio of seawater.

Relatively minimal susceptibility of primary benthic foraminiferal $\delta^{18}O$ values in pelagic sediments towards diagenesis has been noted in previous studies (Edgar et al., 2013; Voigt et al., 2016). These authors attribute the robustness of benthic foraminiferal $\delta^{18}O$ values to diagenetic alteration occurring dominantly at shallow burial depths (<100 m) and very rapidly after deposition (<100 kyr) in a recrystallization environment similar to that of initial calcification. Their scenario of shallow diagenesis is supported by numerical modeling (e.g., Rudnicki et al., 2001). Additional complications can arise in settings with very low sedimentation rates and/or an overlying hiatus, where benthic foraminiferal $\delta^{18}O$ values can become severely altered (Sexton and Wilson, 2009).

None of the sites investigated in this study are marked by very low sedimentation rates or an overlying hiatus (Table 1). However, our modeled initial benthic foraminiferal calcification temperatures for different fractions of secondary inorganic calcite at Sites 1260 and 1263 (Fig. 8) indicate that, even in the case of shallow diagenesis, benthic foraminiferal $\delta^{18}O$ values and the resulting paleotemperatures can potentially be biased, depending on the amount of secondary inorganic calcite added, pore fluid chemistry and the rate of inorganic calcite precipitation. Modeled primary foraminiferal $\delta^{18}O$ (and $\delta^{13}C$) signatures for different fractions of diagenetic calcite are shown in Fig. S13.
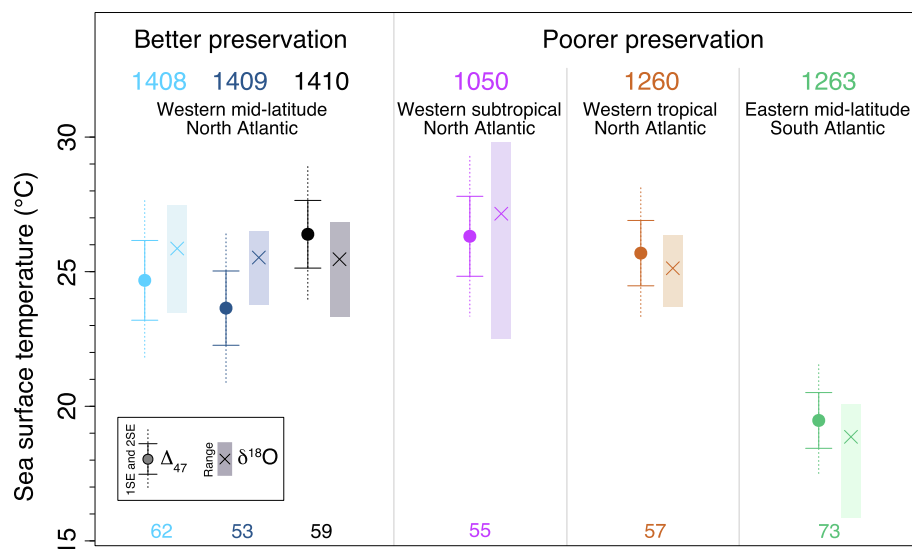
Fig. 7. Planktic Δ_{47}-based (circles) and δ^{18}O-based (crosses) temperatures averaged over the overlapping time interval (illustrated in Fig. 5). The study sites from different oceanographic regimes are characterized by a wide range of preservation states. ±1SE and ±2SE of Δ_{47}-based temperatures are depicted by solid and dotted lines, respectively. Shaded bars show value ranges of δ^{18}O-based temperatures. The number of measurements used for the calculation of the clumped isotope temperature values are listed at the bottom of the plots.

The temperature-dependence for ^{18}O uptake proposed by Watkins et al. (2013) is assumed to describe ^{18}O fractionation for slow inorganic calcite precipitation under near-equilibrium conditions, whereas the temperature-dependence proposed by Kim and O'Neil (1997) has been recently shown to reflect inorganic calcite growth rates, which are too high for isotopic equilibrium (Watkins et al., 2014). When using the fractionation factor of Watkins et al. (2013) for diagenetic calcite, our two-component mixing model indicates a potentially high susceptibility of δ^{18}O-based paleotemperatures towards diagenesis (neomorphism and cementation), even in benthic foraminifera, with a bias of up to 2.0 °C for 20% diagenetic calcite and up to 8.0 °C for 50% diagenetic calcite (Fig. 8a). In the non-equilibrium regime described by Kim and O'Neil (1997), the bias is found to be significantly smaller (<1.0 °C for up to 50% diagenetic calcite).

We propose two possible explanations for the observed robustness of benthic foraminiferal δ^{18}O towards diagenesis: (1) Benthic foraminiferal tests at Sites 1260 and 1263 are generally unsusceptible to neomorphism, owing to their denser tests and their higher resistance to dissolution in comparison to planktic foraminiferal tests (e.g., Berger, 1973; Pearson et al., 2001). Therefore, contributions of secondary calcite during post-depositional diagenesis are minor. Although there is clear visible evidence for cementation with overgrowths of diagenetic calcite, in mass balance terms, this might be a proportionally minor component of whole test calcite, resulting in negligible δ^{18}O shifts of whole test δ^{18}O compositions. (2) Rates of inorganic calcite precipitation in sedimentary pore waters are too fast for isotopic equilibrium, e.g., as described by the equation of Kim and O'Neil (1997), and the fractionation of oxygen isotopes between inorganic calcite and water is similar to the fractionation in modern benthic foraminifera such as Cibicidoides spp. (the calibration equation used for Cibici-

doides (Eq. (1), Bemis et al., 1998) and the inorganic calcite equation of Kim and O'Neil (1997) agree well, as documented in Bemis et al. (1998)). Together with our assumption of shallow burial diagenesis, this second potential explanation implies similar precipitation temperatures and δ^{18}O signatures of benthic foraminiferal (primary) and inorganic (secondary) calcites, and correspondingly small changes in benthic foraminiferal δ^{18}O through neomorphism and cementation. Our two explanations are not mutually exclusive. In fact, it is likely that the small impact of diagenesis on benthic foraminiferal δ^{18}O is caused by some combination of test robustness and inorganic calcite growth rates that are faster than those in equilibrium.

To the best of our knowledge, the sensitivity of primary Δ_{47} signatures of benthic foraminiferal tests to diagenetic alteration has not yet been tested. Our Δ_{47} results suggest no significant effect on benthic foraminiferal Δ_{47} values and DSTs derived therefrom (Figs. 4d and 6a). Isotope exchange reactions within carbonates as well as between carbonates and surrounding fluids seem to be of minor importance for isotope ordering of these calcites. This is in line with the view that C-O bond reordering in the solid mineral lattice of primary calcites is not substantial at burial temperatures below 100 °C for timescales from 10^6 to 10^8 years (Henkes et al., 2014). We show here that this holds true even in natural environments where the primary calcite is in permanent or semipermanent contact with water.

Similarly, our end-member modeling also suggests that clumped isotope paleotemperatures based on benthic foraminiferal Δ_{47} values are relatively insensitive to diagenetic processes such as neomorphism and cementation (bias of <1.2 °C for up to 50% diagenetic calcite), due to our assumption that DSTs can be used to approximate diagenetic calcite precipitation temperatures in a scenario of shallow burial diagenesis (Fig. 8b). We include two scenarios of deep diagenesis where diagenetic alteration occurs
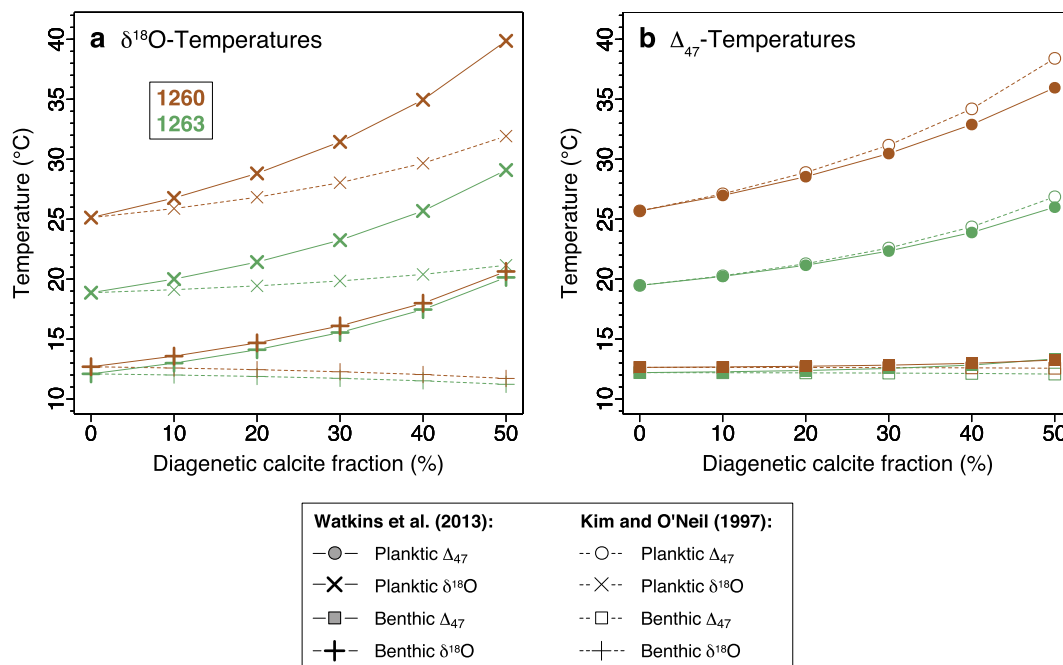
Fig. 8. Temperatures of initial biogenic calcification calculated for various assumed percentages of early diagenetic inorganic calcite at Sites 1260 (red) and 1263 (green). SEM images suggest substantial fractions of diagenetic calcite at Sites 1260 and 1263, in contrast to Site 1409. At the same time, both planktic and benthic isotope data are available at Sites 1260 and 1263. Panel (a) shows $\delta^{18}O$-based temperatures from planktic (crosses) and benthic (plus signs) foraminifera, whereas the values shown in (b) are based on the Δ_{47} signatures of planktic (circles) and benthic (squares) foraminifera. Starting points of the curves are the temperatures calculated from measured Δ_{47} and $\delta^{18}O$ (i.e., diagenetic calcite fraction = 0%). Calculations were performed using both the fractionation factor of Watkins et al. (2013) (solid lines) and the fractionation factor of Kim and O'Neil (1997) (dashed lines) for inorganic calcite.

near final burial depths (Fig. S14). In these cases, DSTs derived from $\delta^{18}O$ and Δ_{47} signatures of benthic foraminiferal tests may be biased to a larger degree, depending on pore fluid chemistry (Fig. S15). For example, the modeled diagenetic bias in foraminiferal Δ_{47}-based DSTs at Site 1260 is +3.2 °C, when assuming an extreme case of deep diagenesis near final burial depths under a middle Eocene geothermal gradient of 30 °C/km, 50% diagenetic calcite and ^{18}O fractionation during diagenetic calcite precipitation according to Watkins et al. (2013). However, our extreme scenarios of deep diagenesis are considered unlikely, based on numerical modeling and empirical data (e.g., Rudnicki et al., 2001; Edgar et al., 2013; Voigt et al., 2016), and should be seen as a sensitivity experiment only. We further note that effects on Δ_{47} values purely from dissolution have not yet been investigated.

5.2. Robustness of Δ_{47}- and $\delta^{18}O$-based sea surface temperature reconstructions

$\delta^{18}O$ signatures of shallow-dwelling planktic foraminifera are thought to be more susceptible to diagenesis than those of benthic foraminifera, primarily because of the contrast in carbonate precipitation environments (e.g., temperature, pH) between upper water column and bottom waters or sedimentary pore fluids (e.g., Edgar et al., 2013). Mean tropical SST values derived from frosty planktic foraminiferal $\delta^{18}O$ and Δ_{47} signatures are lower than 26 °C at tropical West Atlantic Site 1260 (Fig. 7). These reconstructed

tropical SST values are thus substantially lower than previous middle Eocene (42–46 Ma) SST estimates of approximately 30–34 °C for other parts of the tropics (Evans et al., 2018). Moreover, they are similar to our $\delta^{18}O$- and Δ_{47}-based SST values from Sites 1408, 1409, 1410 and 1050 located at higher northern latitudes. Although we cannot exclude additional factors, such as differences in seasonality between the sites, we interpret the observed similarities between tropical and higher latitude SST values as primarily caused by partial diagenetic overprinting of tropical SST signatures in colder pore fluids.

End-member modeling supports this interpretation, indicating significant susceptibility of planktic foraminiferal calcite to diagenesis, both in terms of Δ_{47} and $\delta^{18}O$ values (Fig. 8). For Site 1260 in the tropical West Atlantic, our model calculations based on the assumptions listed in Table 2 and the ^{18}O fractionation factor of Watkins et al. (2013) indicate that assuming an inorganic calcite fraction of 20% would lead to a cold bias of −2.9 °C in SST derived from Δ_{47}, while a fraction of 50% would result in a bias of −10.3 °C. Using the fractionation factor of Kim and O'Neil (1997) to calculate inorganic calcite $\delta^{18}O$ compositions from pore fluid $\delta^{18}O$ values, we obtain similar cold biases for Δ_{47}-based SSTs amounting to −3.2 and −12.7 °C for 20 and 50% inorganic calcite, respectively. For $\delta^{18}O$-based SSTs, inorganic calcite fractions of 20 and 50% result in cold biases of −3.7 and −14.7 °C, when using the fractionation factor of Watkins et al. (2013), but only −1.7 and −6.8 °C, when using the factor of Kim and O'Neil

(1997). For comparison, Pearson et al. (2001) suggested that tropical SSTs derived from the $\delta^{18}O$ composition of planktic foraminiferal tests with 50% diagenetic calcite may be underestimated by roughly 10–15 °C.

In comparison to the tropics, the modeled effect of diagenetic alteration on stable isotopes in fossil planktic foraminiferal tests from middle latitudes is more modest (Fig. 8), due to smaller differences in isotopic composition between planktic foraminiferal and inorganic calcite (Fig. 5 and Table 2). For Δ_{47}-based SSTs at Site 1263 in the southern mid-latitude East Atlantic, cold biases calculated with the ^{18}O fractionation factor of Watkins et al. (2013) amount to −1.7 °C and −6.5 °C for inorganic calcite contributions of 20 and 50%, respectively. The values based on the factor of Kim and O'Neil (1997) are relatively similar at this site (−1.8 °C and −7.4 °C for 20% and 50%). For $\delta^{18}O$-based SSTs, modeled cold bias values diverge substantially when using different fractionation factors to calculate inorganic calcite $\delta^{18}O$, similar as observed for Site 1260 in the tropics, ranging from −0.6 °C to −2.6 °C for 20% inorganic calcite and from −2.3 °C to −10.2 °C for 50% inorganic calcite.

Because of their strong dependence on the $\delta^{18}O$ composition of pore fluids and inorganic calcite precipitated therefrom, the sensitivities of $\delta^{18}O$-based SSTs to diagenetic alteration are more uncertain than those of Δ_{47}-based SSTs. Our estimates for inorganic calcite $\delta^{18}O$ and $\delta^{13}C$ signatures (Table 2) are in the range of the values reported in previous studies (e.g., Pearson et al., 2001; Sexton and Wilson, 2009; Voigt et al., 2016). However, $\delta^{18}O$ and $\delta^{13}C$ compositions of diagenetic inorganic calcite are relatively poorly constrained in these and in our study, owing to a lack of direct measurements (e.g., acquired by in situ secondary ion mass spectrometry (SIMS) as documented in Kozdon et al. (2013)). Inorganic calcite $\delta^{18}O$, $\delta^{13}C$ and Δ_{47} values may be affected by "closed" system effects (i.e., limited exchange with pore fluids) and/or non-equilibrium isotope fractionation varying with salinity, pH and/or crystal growth rate (e.g., Hill et al., 2014; Watkins et al., 2014). Using the ^{18}O fractionation factor of Kim and O'Neil (1997) instead of Watkins et al. (2013) for inorganic calcite significantly lowers the sensitivity of foraminiferal $\delta^{18}O$ signatures to diagenetic alteration. In comparison, changing the ^{18}O fractionation factor has only a slight influence on the sensitivity of foraminiferal Δ_{47} values to diagenesis (due to different diagenetic end-member $\delta^{18}O$ compositions affecting non-linear mixing of Δ_{47}).

Furthermore, we note that if a simpler mixing model is used for estimating the effects of diagenesis on Δ_{47}, which does not consider non-linear mixing effects, then the modeled diagenetic effects would be larger. In this case, assuming 20% and 50% inorganic calcite result in cold biases of −3.5 °C and −14.6 °C at Site 1260 and −1.8 °C and −7.5 °C at Site 1263 (see Fig. S16 for a comparison between linear and non-linear Δ_{47} mixing). The magnitudes of these values are independent of the ^{18}O fractionation factor. The comparison between linear and non-linear mixing modeling demonstrates that the bias of Δ_{47}-based primary SST signals by diagenetic overprinting is partially mitigated by non-linear Δ_{47} mixing effects, which are caused by differences between the end-member isotopic compositions

(e.g., Defliese and Lohmann, 2015). Thereby, the mixing offset is larger for large differences in $\delta^{18}O$ and/or $\delta^{13}C$ between the end-member compositions in comparison to small differences. Assuming small fractions of diagenetic calcite (20% and below), non-linear mixing effects on clumped isotope SST values appear generally small (<1 °C). For larger fractions of inorganic calcite, however, mitigation of diagenetic overprinting by non-linear mixing effects can be substantial in some settings. At Site 1260 in the tropics, for example, non-linear mixing effects reduce the modeled SST cold bias by 4.4 °C, when assuming an inorganic calcite fraction of 50% and equilibrium fractionation of ^{18}O in inorganic calcite (described by the ^{18}O fractionation factor of Watkins et al. (2013)).

We conducted a range of sensitivity analyses for different values of inorganic calcite $\delta^{18}O$ and $\delta^{13}C$ (Figs. S17 and S18). As expected, the sensitivity of Δ_{47}-derived paleotemperatures to diagenetic alteration is less affected by different values for inorganic calcite $\delta^{18}O$ in comparison to the sensitivity of $\delta^{18}O$-derived paleotemperatures, which even changes sign (Fig. S17). This makes it more difficult to correct paleotemperatures derived from the $\delta^{18}O$ signatures of foraminiferal tests for diagenetic alteration. Furthermore, utilizing mean planktic foraminiferal $\delta^{13}C$ values measured at each site (3.3‰ and 2.9‰ at Sites 1260 and 1263, respectively) instead of bulk $\delta^{13}C$ values (Table 2) to approximate inorganic calcite $\delta^{13}C$ values increases the sensitivity of Δ_{47}-based SSTs to diagenesis from 0.0 °C to 0.7 °C for 20% inorganic calcite and from 0.3 °C to 5.0 °C for 50% inorganic calcite, due to a weakening of non-linear mixing effects (Fig. S18). In contrast, inorganic calcite $\delta^{13}C$ values that are lower than bulk $\delta^{13}C$ (e.g., caused by organic carbon degradation) lead to stronger non-linear mixing effects and thus decreased sensitivity of primary Δ_{47} signatures to diagenetic alteration. Furthermore, diagenesis at deeper burial depths would imply a generally smaller cool bias in $\delta^{18}O$- and Δ_{47}-based SST values reconstructed from altered planktic foraminiferal tests (Figs. S14 and S15) than shallow diagenesis (shown in Fig. 8).

Comparison of samples from the clay-rich sedimentary sequences of Sites 1408, 1409 and 1410 provides an opportunity to assess if whole test $\delta^{18}O$ and Δ_{47} compositions of planktic foraminifera may be affected by the presence of very minor overgrowths of diagenetic calcite even in locations with generally good preservation of foraminifera (Fig. 3). Owing to the very close proximity of these Newfoundland sites to each other, planktic foraminiferal tests are assumed to reflect similar surface water conditions. In comparison to Site 1409, middle Eocene sediments at Sites 1408 and 1410 were deposited more rapidly and are more deeply buried (Table 1). After deposition, foraminiferal tests at Site 1409 thus stayed comparably long at shallow depths, where diffusive fluxes in pore fluids and reactive rates tend to be highest (e.g., Edgar et al., 2013). However, SEM images indicate only minor differences in preservation (Fig. 3), suggesting that these contrasting sedimentological facets of Sites 1408 and 1410 versus 1409 had minimal impact on differential diagenetic alteration.

In our isotope data, we find no evidence that Sites 1408, 1409 and/or 1410 might have been significantly affected by

diagenesis. Averages and ranges of δ^{18}O-based SST values are similar at Sites 1408, 1409 and 1410 (Fig. 7). Planktic foraminiferal δ^{13}C values at Sites 1408, 1409 and 1410 are also in good agreement with each other (Fig. S11b). The observed range (~3 °C) among the average clumped isotope temperature results from Sites 1408, 1409 and 1410 is likely attributable to analytical uncertainties. Our findings imply that non-glassy planktic foraminiferal tests with minor signs of diagenetic calcite overgrowths but without visible neomorphism can be confidently used for δ^{18}O- and Δ_{47}-based paleoclimate reconstructions.

5.3. Comparison with other estimates for middle Eocene temperatures

Fig. 9 shows the clumped isotope temperature estimates from this study plotted with existing SST and DST recon-
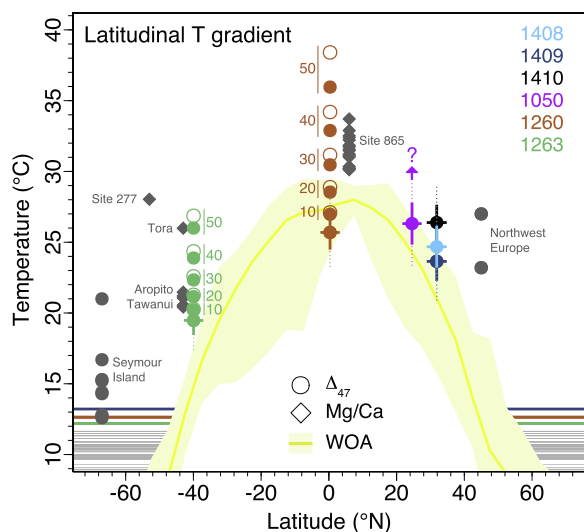

Fig. 9. Middle Eocene (42–46 Ma) SSTs and DSTs based on Δ_{47} and Mg/Ca compared to modern mean annual temperatures from the World Ocean Atlas 2013 (WOA, yellow, Locarnini et al., 2013). Reconstructed SST values from this study (circles) are shown with uncertainties (vertical solid lines = $\pm$1SE, vertical dotted lines = $\pm$2SE, horizontal solid lines = uncertainty in paleolatitude according to van Hinsbergen et al. (2015)). The Δ_{47}-based SST values derived from the frosty foraminiferal tests at Sites 1050, 1260 and 1263 are likely too low. Therefore, the range of SST values is illustrated for inorganic calcite fractions of 10, 20, 30, 40 and 50% for Sites 1260 and 1263. These values were calculated using either the ^{18}O fractionation factor of Watkins et al. (2013) (filled circles) or that of Kim and O'Neil (1997) (open circles). Mg/Ca SSTs (dark gray diamonds) from DSDP Site 277 as well as the localities Aropito, Tawanui and Tora in the Southwest Pacific area (Hines et al., 2017) and Site 865 in the equatorial Pacific (Tripati et al., 2003) were reevaluated by Evans et al. (2018). Dark gray circles are clumped isotope-based estimates from shallow-dwelling benthic foraminifera in Northwest Europe (Evans et al., 2018) and from bivalve shells from Seymour Island in the South Pacific (Douglas et al., 2014). Horizontal lines show DSTs measured in this study and the reconstruction of Cramer et al. (2011) for the interval from 42 to 46 Ma (light gray). Zonal mean and range in WOA SST (data from https://www.nodc.noaa.gov/cgi-bin/OC5/woa13/woa13.pl) are depicted by yellow lines and shading, respectively.

structions from 42 to 46 Ma (Evans et al., 2018), representing an interval without major transitions or perturbations in global climate (e.g., Sexton et al., 2006a; Zachos et al., 2008). SST estimates based on foraminiferal δ^{18}O values are not shown, owing to their dependence on poorly constrained seawater δ^{18}O. Mg/Ca-based SST values were compiled and recalculated by Evans et al. (2018), using seawater Mg/Ca data derived from the Δ_{47} and Mg/Ca signatures of shallow-dwelling large benthic foraminifera. In addition, we compare to clumped isotope SSTs derived from bivalve shells from Seymour Island, located in the South Pacific near the Antarctic Peninsula (Douglas et al., 2014).

Δ_{47}-derived SST estimates from frosty foraminifera at Sites 1260 and 1263 are cooler than existing Mg/Ca-based SST values for similar paleolatitudes. The apparent cool bias at Site 1260 would be greatly reduced when correcting for secondary inorganic calcite fractions from 10 to 50%. For example, our Δ_{47}-based SST estimate corrected for 30–40% inorganic calcite at Site 1260 is in excellent agreement with Mg/Ca-based SSTs from ODP Site 865 in the western central equatorial Pacific (Tripati et al., 2003; Evans et al., 2018). The observed offset between SST values from Site 1263 in the eastern South Atlantic and DSDP Site 277 in the Southwest Pacific Ocean as well as the localities Aropito, Tawanui and Tora in eastern New Zealand (Hines et al., 2017; Evans et al., 2018) may be linked to differences in foraminiferal preservation and/or oceanographic regime between these distant sites. Given that Site 1263 is located near the eastern boundary of an ocean basin, comparably low SSTs at this site could have been caused by upwelling of cooler waters. However, low sedimentation rates observed at Site 1263 (Table 1) may indicate that there was no major upwelling at this site in the past, and the observed overgrowth on foraminifera used in this study does suggest that the colder temperature is at least in part due to diagenetic alteration. For Site 1050, the sensitivity of the SST value to diagenetic alteration was not modeled, as no benthic foraminiferal data were available to estimate the isotopic composition of inorganic calcite at this site. The uncorrected clumped isotope SST estimate for Site 1050 is likely too low, based on our assessment of planktic foraminiferal preservation at this site. In contrast, our new SST estimates derived from the well-preserved foraminiferal tests at Newfoundland Sites 1408, 1409 and 1410 indicate reasonable temperatures for the mid-latitudes, which were warmer than present during the middle Eocene greenhouse (Fig. 9).

Clumped isotope DSTs from Sites 1409, 1260 and 1263 appear higher (+0.6–4.3 °C) than the Mg/Ca-based DST values from the global compilation of Cramer et al. (2011). Mg/Ca DSTs (42–46 Ma) have been calculated by Cramer et al. (2011) based on seawater Mg/Ca values that are in good agreement with recent estimates for the middle Eocene (Evans et al., 2018), and have thus not been updated here. The offset observed between Δ_{47}-derived and Mg/Ca-derived DSTs may however be explainable by calibration uncertainty and/or possible vital effects in foraminiferal Mg/Ca compositions as well as inter-basin differences in DST and/or carbonate chemistry effects (e.g.,

saturation state) biasing Mg/Ca-based DSTs towards lower temperatures (e.g., Lear et al., 2010).

6. CONCLUSIONS

We used middle Eocene benthic and planktic foraminifera from six ODP/IODP sites in the Atlantic Ocean to test the effects of diagenesis on the stable and clumped isotopic compositions of foraminiferal calcites. SEM images revealed significant differences in carbonate fossil preservation between the sites. The clay-rich sediments from the Newfoundland Drifts host exceptionally well-preserved foraminiferal tests, whereas foraminifera from the more carbonate-rich pelagic settings, commonly used for Paleogene climate reconstructions, are characterized by poorer preservation states with clear diagenetic features. However, despite different burial histories and variable foraminiferal preservation, inter-site offsets in $\delta^{18}O$- and Δ_{47}-based DSTs from benthic foraminifera at the sites examined are negligible. Hence, primary benthic $\delta^{18}O$ and Δ_{47} signatures seem generally well preserved during post-depositional diagenesis under the conditions and timescales represented by our study sites. On the other hand, planktic foraminiferal tests from the carbonate-rich sediments showed clear signs of alteration. $\delta^{18}O$ and Δ_{47} compositions of these planktic tests both yield SSTs that are cooler than expected. The cool bias appears to be most pronounced at tropical Site 1260, and less so at mid-latitude Sites 1050 and 1263. This finding is consistent with our end-member mixing model results, which indicate that the susceptibility of planktic isotopic signatures to post-depositional alteration (neomorphism and cementation) is most visible in the tropics (where the seafloor temperatures under which diagenetic alteration occurs are most different from those of the overlying surface ocean where the planktic foraminifera lived). We furthermore find that diagenetic overprinting of primary Δ_{47} signals can be partially mitigated by non-linear Δ_{47} mixing effects, with the extent of this mitigating effect ranging from negligible to substantial depending on the setting and extent of overprinting. $\delta^{18}O$ and Δ_{47} compositions of the well-preserved planktic foraminiferal tests from the clay-rich sediments at Sites 1408, 1409 and 1410 located on Newfoundland Rise yield SST values with minimal impact of diagenetic alteration, despite slightly different burial histories.

In summary, we show that benthic foraminifera from deep-sea sediments and well preserved planktic foraminifera from clay-rich sediments may be used for $\delta^{18}O$- and Δ_{47}-based ocean temperature reconstructions, whereas SST reconstructions from planktic foraminiferal tests deposited in carbonate-rich settings can be compromised by diagenetic alteration, particularly in the tropics. We do not observe additional diagenetic effects altering Δ_{47} values beyond the effect of adding/replacing calcite at temperatures encountered in the deep-sea at the sites studied here. Rather, Δ_{47}-based SSTs are found to be similarly susceptible to diagenesis as those based on $\delta^{18}O$, with differences mostly depending on pore water chemistry and the amount of secondary inorganic calcite in a foraminiferal test. In the future, a means of estimating the percentage of inorganic calcite in fossil foraminiferal tests (e.g., by EBSD) would enable correction of planktic foraminiferal Δ_{47} (and to a lesser extent $\delta^{18}O$) signatures for post-depositional alteration, based on benthic Δ_{47} values and the modeling approach shown in this study. This approach offers paleoceanographers the potential to derive more accurate SST values from diagenetically altered planktic foraminifera.

APPENDIX A. SUPPLEMENTARY MATERIAL

Supplementary data to this article can be found online at https://doi.org/10.1016/j.gca.2019.05.005.

REFERENCES

Bemis B. E., Spero H. J., Bijma J. and Lea D. W. (1998) Reevaluation of the oxygen isotopic composition of planktonic foraminifera: Experimental results and revised paleotemperature equations. *Paleoceanography* **13**, 150–160.

Berger W. H. (1973) Deep-sea carbonates: pleistocene dissolution cycles. *J. Foramin. Res.* **3**, 187–195.

Bernasconi S. M., Müller I. A., Bergmann K. D., Breitenbach S. F. M., Fernandez A., Hodell D. A., Jaggi M., Meckler A. N., Millan I. and Ziegler M. (2018) Reducing uncertainties in carbonate clumped isotope analysis through consistent carbonate-based standardization. *Geochem. Geophys. Geosyst.* **19**, 2895–2914.

Boulila S., Vahlenkamp M., De Vleeschouwer D., Laskar J., Yamamoto Y., Pälike H., Kirtland Turner S., Sexton P. F., Westerhold T. and Röhl U. (2018) Towards a robust and consistent middle Eocene astronomical timescale. *Earth Planet. Sci. Lett.* **486**, 94–107.

Boyle P. R., Romans B. W., Tucholke B. E., Norris R. D., Swift S. A. and Sexton P. F. (2017) Cenozoic North Atlantic deep circulation history recorded in contourite drifts, offshore Newfoundland, Canada. *Mar. Geol.* **385**, 185–203.

Breitenbach S. F. M., Mleneck-Vautravers M. J., Grauel A.-L., Lo L., Bernasconi S. M., Müller I. A., Rolfe J., Gázquez F., Greaves M. and Hodell D. A. (2018) Coupled Mg/Ca and clumped isotope analyses of foraminifera provide consistent water temperatures. *Geochim. Cosmochim. Acta* **236**, 283–296.

Brown S. J. and Elderfield H. (1996) Variations in Mg/Ca and Sr/Ca ratios of planktonic foraminifera caused by postdepositional dissolution: Evidence of shallow Mg-dependent dissolution. *Paleoceanography* **11**, 543–551.

Cramer B. S., Miller K. G., Barrett P. J. and Wright J. D. (2011) Late Cretaceous-Neogene trends in deep ocean temperature and continental ice volume: Reconciling records of benthic foraminiferal geochemistry ($\delta^{18}O$ and Mg/Ca) with sea level history. *J. Geophys. Res.-Oceans* **116**, 1–23.

Crowley T. J. and Zachos J. C. (1999) Comparison of zonal temperature profiles for past warm time periods. In *Warm Climates in Earth History* (eds. B. Huber, K. Macleod and S. Wing). Cambridge University Press, New York, pp. 50–76.

Defliese W. F. and Lohmann K. C. (2015) Non-linear mixing effects on mass-47 CO_2 clumped isotope thermometry: Patterns and implications. *Rapid Commun. Mass Spectrom.* **29**, 901–909.

Delaney M. L. (1989) Temporal Changes in Interstitial Water Chemistry and Calcite Recrystallization in Marine Sediments. *Earth Planet. Sci. Lett.* **95**, 23–37.

Dhondt S. and Arthur M. A. (1996) Late cretaceous oceans and the cool tropic paradox. *Science* **271**, 1838–1841.

Douglas P. M. J., Affek H. P., Ivany L. C., Houben A. J. P., Sijp W. P., Sluijs A., Schouten S. and Pagani M. (2014) Pronounced zonal heterogeneity in Eocene southern high-latitude sea surface temperatures. *PNAS* **111**, 6582–6587.

Edgar K. M., Anagnostou E., Pearson P. N. and Foster G. L. (2015) Assessing the impact of diagenesis on $\delta^{11}B$, $\delta^{13}C$, $\delta^{18}O$, Sr/Ca and B/Ca values in fossil planktic foraminiferal calcite. *Geochim. Cosmochim. Acta* **166**, 189–209.

Edgar K. M., Pälike H. and Wilson P. A. (2013) Testing the impact of diagenesis on the $\delta^{18}O$ and $\delta^{13}C$ of benthic foraminiferal calcite from a sediment burial depth transect in the equatorial Pacific. *Paleoceanography* **28**, 468–480.

Edgar K. M., Wilson P. A., Sexton P. F. and Suganuma Y. (2007) No extreme bipolar glaciation during the main Eocene calcite compensation shift. *Nature* **448**, 908–911.

Eiler J. M. and Schauble E. (2004) $^{18}O^{13}C^{16}O$ in Earth's atmosphere. *Geochim. Cosmochim. Acta* **68**, 4767–4777.

Erbacher, J., Mosher, D.C., Malone, M.J. and the Expedition 207 Scientists (2004) Site 1260, Proceedings of the Ocean Drilling Program, Initial Reports Volume 207, pp. 1–113.

Evans D., Sagoo N., Renema W., Cotton L. J., Muller W., Todd J. A., Saraswati P. K., Stassen P., Ziegler M., Pearson P. N., Valdes P. J. and Affek H. P. (2018) Eocene greenhouse climate revealed by coupled clumped isotope-Mg/Ca thermometry. *PNAS* **115**, 1174–1179.

Fantle M. S. and DePaolo D. J. (2007) Ca isotopes in carbonate sediment and pore fluid from ODP Site 807A: The Ca^{2+}(aq)-calcite equilibrium fractionation factor and calcite recrystallization rates in Pleistocene sediments. *Geochim. Cosmochim. Acta* **71**, 2524–2546.

Fernandez A., Müller I. A., Rodríguez-Sanz L., van Dijk J., Looser N. and Bernasconi S. M. (2017) A reassessment of the precision of carbonate clumped isotope measurements: implications for calibrations and paleoclimate reconstructions. *Geochem. Geophys. Geosyst.* **18**, 4375–4386.

Ghosh P., Adkins J., Affek H., Balta B., Guo W., Schauble E. A., Schrag D. and Eiler J. M. (2006) $^{13}C–^{18}O$ bonds in carbonate minerals: A new kind of paleothermometer. *Geochim. Cosmochim. Acta* **70**, 1439–1456.

Golreihan A., Steuwe C., Woelders L., Deprez A., Fujita Y., Vellekoop J., Swennen R. and Roeffaers M. B. J. (2018) Improving preservation state assessment of carbonate microfossils in paleontological research using label-free stimulated Raman imaging. *PLoS ONE* **13**, 1–15.

Grauel A. L., Schmid T. W., Hu B., Bergami C., Capotondi L., Zhou L. and Bernasconi S. M. (2013) Calibration and application of the 'clumped isotope' thermometer to foraminifera for high resolution climate reconstructions. *Geochim. Cosmochim. Acta* **108**, 125–140.

Henkes G. A., Passey B. H., Grossman E. L., Shenton B. J., Perez-Huerta A. and Yancey T. E. (2014) Temperature limits for preservation of primary calcite clumped isotope paleotemperatures. *Geochim. Cosmochim. Acta* **139**, 362–382.

Henkes G. A., Passey B. H., Grossman E. L., Shenton B. J., Yancey T. E. and Perez-Huerta A. (2018) Temperature evolution and the oxygen isotope composition of Phanerozoic oceans from carbonate clumped isotope thermometry. *Earth Planet. Sci. Lett.* **490**, 40–50.

Hill P. S., Tripati A. K. and Schauble E. A. (2014) Theoretical constraints on the effects of pH, salinity, and temperature on clumped isotope signatures of dissolved inorganic carbon species and precipitating carbonate minerals. *Geochim. Cosmochim. Acta* **125**, 610–652.

Hines B. R., Hollis C. J., Atkins C. B., Baker J. A., Morgans H. E. G. and Strong P. C. (2017) Reduction of oceanic temperature gradients in the early Eocene Southwest Pacific Ocean. *Palaeogeogr. Palaeoclimatol. Palaeoecol.* **475**, 41–54.

Hu B., Radke J., Schlüter H. J., Heine F. T., Zhou L. and Bernasconi S. M. (2014) A modified procedure for gas-source isotope ratio mass spectrometry: the long-integration dual-inlet (LIDI) methodology and implications for clumped isotope measurements. *Rapid Commun. Mass Spectrom.* **28**, 1413–1425.

Hull, P.M., Bohaty, S.M., Cameron, A., Coxall, H.K., D'haenens, S., De Vleeschouwer, D., Elder, L.E., Friedrich, O., Kerr, K., Turner, S.K., Kordesch, W.E.C., Moriya, K., Norris, R.D., Opdyke, B.N., Penman, D.E., Pälike, H., Wilson, P.A., Sexton, P.F., Vahlenkamp, M., Wu, F. and Zachos, J.C., 2017. Data report: coarse fraction record for the Eocene megasplice at IODP Sites U1406, U1408, U1409, and U1411, Norris, R.D., Wilson, P.A., Blum, P., and the Expedition 342 Scientists, Proc. IODP, 342: College Station, TX (Integrated Ocean Drilling Program).

Huntington K. W., Eiler J. M., Affek H. P., Guo W., Bonifacie M., Yeung L. Y., Thiagarajan N., Passey B. H., Tripati A. K., Daeron M. and Came R. (2009) Methods and limitations of 'clumped' CO_2 isotope (Δ_{47}) analysis by gas-source isotope ratio mass spectrometry. *J. Mass Spectrom.* **44**, 1318–1329.

John C. M. and Bowen D. (2016) Community software for challenging isotope analysis: First applications of 'Easotope' to clumped isotopes. *Rapid Commun. Mass Spectrom.* **30**, 2285–2300.

Katz M. E., Katz D. R., Wright J. D., Miller K. G., Pak D. K., Shackleton N. J. and Thomas E. (2003) Early Cenozoic benthic foraminiferal isotopes: Species reliability and interspecies correction factors. *Paleoceanography* **18**.

Kele S., Breitenbach S. F. M., Capezzuoli E., Meckler A. N., Ziegler M., Millan I. M., Kluge T., Deák J., Hanselmann K., John C. M., Yan H., Liu Z. and Bernasconi S. M. (2015) Temperature dependence of oxygen- and clumped isotope fractionation in carbonates: A study of travertines and tufas in the 6–95 °C temperature range. *Geochim. Cosmochim. Acta* **168**, 172–192.

Killingley J. S. (1983) Effects of diagenetic recrystallization on $^{18}O/^{16}O$ values of deep-sea sediments. *Nature* **301**, 594–597.

Kim S. T. and O'Neil J. R. (1997) Equilibrium and nonequilibrium oxygen isotope effects in synthetic carbonates. *Geochim. Cosmochim. Acta* **61**, 3461–3475.

Kozdon R., Kelly D. C., Kita N. T., Fournelle J. H. and Valley J. W. (2011) Planktonic foraminiferal oxygen isotope analysis by

ion microprobe technique suggests warm tropical sea surface temperatures during the Early Paleogene. *Paleoceanography* **26**.

Kozdon R., Kelly D. C., Kitajima K., Strickland A., Fournelle J. H. and Valley J. W. (2013) In situ $\delta^{18}O$ and Mg/Ca analyses of diagenetic and planktic foraminiferal calcite preserved in a deep-sea record of the Paleocene-Eocene thermal maximum. *Paleoceanography* **28**, 517–528.

Laskar J., Fienga A., Gastineau M. and Manche H. (2011a) La2010: a new orbital solution for the long-term motion of the Earth. *Astron. Astrophys.* **532**.

Laskar J., Gastineau M., Delisle J.-B., Farrés A. and Fienga A. (2011b) Strong chaos induced by close encounters with Ceres and Vesta. *Astron. Astrophys.* **532**.

Laskar J., Robutel P., Joutel F., Gastineau M., Correia A. C. M. and Levrard B. (2004) A long-term numerical solution for the insolation quantities of the Earth. *Astron. Astrophys.* **428**, 261–285.

Lear Caroline H., Mawbey Elaine M. and Rosenthal Yai (2010) Cenozoic benthic foraminiferal Mg/Ca and Li/Ca records: Toward unlocking temperatures and saturation states. *Paleoceanography* **25**.

Locarnini, R.A., Mishonov, A.V., Antonov, J.I., Boyer, T.P., Garcia, H.E., Baranova, O.K., Zweng, M.M., Paver, C.R., Reagan, J.R., Johnson, D.R., Hamilton, M., Seidov, D., 2013. World Ocean Atlas 2013, Volume 1: Temperature. S. Levitus, Ed., A. Mishonov Technical Ed. NOAA Atlas NESDIS 73, 40.

Meckler A. N., Ziegler M., Millan M. I., Breitenbach S. F. M. and Bernasconi S. M. (2014) Long-term performance of the Kiel carbonate device with a new correction scheme for clumped isotope measurements. *Rapid Commun. Mass Spectrom.* **28**, 1705–1715.

Müller I. A., Fernandez A., Radke J., van Dijk J., Bowen D., Schwieters J. and Bernasconi S. M. (2017) Carbonate clumped isotope analyses with the long-integration dual-inlet (LIDI) workflow: scratching at the lower sample weight boundaries. *Rapid Commun. Mass Spectrom.* **31**, 1057–1066.

Norris, R.D., Kroon, D., Klaus, A. and the Expedition 171B Scientists (1998) Site 1050, Proceedings of the Ocean Drilling Program, Initial Reports, vol. 171B, pp. 93–169.

Norris, R.D., Wilson, P.A., Blum, P. and the Expedition 342 Scientists (2014a) Site U1408, Proceedings of the Integrated Ocean Drilling Program, volume 342, pp. 1–91.

Norris, R.D., Wilson, P.A., Blum, P. and the Expedition 342 Scientists (2014b) Site U1409, Proceedings of the Integrated Ocean Drilling Program, vol. 342, pp. 1–104.

Norris, R.D., Wilson, P.A., Blum, P. and the Expedition 342 Scientists (2014c) Site U1410, Proceedings of the Integrated Ocean Drilling Program, vol. 342, pp. 1–87.

Ogg J. G. (2012) Chapter 5 – Geomagnetic Polarity Time Scale. In *The Geologic Time Scale* (eds. F. M. Gradstein, J. G. Ogg, M. D. Schmitz and G. M. Ogg). Elsevier, Boston, pp. 85–113.

Ogg, J.G., Bardot, L., 2001. Aptian through Eocene magnetostratigraphic correlation of the Blake Nose Transect (Leg 171B), Florida continental margin, Kroon, D., Norris, R.D., Klaus, A., and the Expedition 171B Scientists, Proc. ODP, 171B, pp. 1–58.

Passey B. H. and Henkes G. A. (2012) Carbonate clumped isotope bond reordering and geospeedometry. *Earth Planet. Sci. Lett.* **351**, 223–236.

Pearson P. N. and Burgess C. E. (2008) Foraminifer test preservation and diagenesis: Comparison of high latitude Eocene sites. *Geol. Soc. Lond. Spec. Publ.* **303**, 59–72.

Pearson P. N., Ditchfield P. W., Singano J., Harcourt-Brown K. G., Nicholas C. J., Olsson R. K., Shackleton N. J. and Hall M. A. (2001) Warm tropical sea surface temperatures in the Late Cretaceous and Eocene epochs. *Nature* **414**, 481–487.

Pearson P. N., Olsson R. K., Huber B. T., Hemleben C., Berggren W. A. and Coxall H. K. (2006) Overview of Eocene Planktonic foraminiferal taxonomy, paleoecology, phylogeny, and biostratigraphy. *Cushman Found. Foraminiferal Res.*, 41.

Peral M., Daëron M., Blamart D., Bassinot F., Dewilde F., Smialkowski N., Isguder G., Bonnin J., Jorissen F., Kissel C., Michel E., Vázquez Riveiros N. and Waelbroeck C. (2018) Updated calibration of the clumped isotope thermometer in planktonic and benthic foraminifera. *Geochim. Cosmochim. Acta* **239**, 1–16.

Piasecki A., Bernasconi S. M., Grauel A. L., Hannisdal B., Ho S. L., Leutert T. J., Marchitto T. M., Meinicke N., Tisserand A. and Meckler A. N. (2019) Application of clumped isotope thermometry to benthic foraminifera. *Geochem. Geophys., Geosyst.* **20**.

Roberts C. D., LeGrande A. N. and Tripati A. K. (2011) Sensitivity of seawater oxygen isotopes to climatic and tectonic boundary conditions in an early Paleogene simulation with GISS ModelE-R. *Paleoceanography* **26**.

Rodríguez-Sanz L., Bernasconi S. M., Marino G., Heslop D., Müller I. A., Fernandez A., Grant K. M. and Rohling E. J. (2017) Penultimate deglacial warming across the Mediterranean Sea revealed by clumped isotopes in foraminifera. *Sci. Rep.* **7**.

Rudnicki M. D., Wilson P. A. and Anderson W. T. (2001) Numerical models of diagenesis, sediment properties, and pore fluid chemistry on a paleoceanographic transect: Blake Nose, Ocean Drilling Program Leg 171B. *Paleoceanography* **16**, 563–575.

Schauble E. A., Ghosh P. and Eiler J. M. (2006) Preferential formation of ^{13}C–^{18}O bonds in carbonate minerals, estimated using first-principles lattice dynamics. *Geochim. Cosmochim. Acta* **70**, 2510–2529.

Schmid T. W. and Bernasconi S. M. (2010) An automated method for 'clumped-isotope' measurements on small carbonate samples. *Rapid Commun. Mass Spectrom.* **24**, 1955–1963.

Schrag D. P. (1999) Effects of diagenesis on the isotopic record of late paleogene tropical sea surface temperatures. *Chem. Geol.* **161**, 215–224.

Sexton P. F., Norris R. D., Wilson P. A., Pälike H., Westerhold T., Röhl U., Bolton C. T. and Gibbs S. (2011) Eocene global warming events driven by ventilation of oceanic dissolved organic carbon. *Nature* **471**, 349–352.

Sexton P. F. and Wilson P. A. (2009) Preservation of benthic foraminifera and reliability of deep-sea temperature records: Importance of sedimentation rates, lithology, and the need to examine test wall structure. *Paleoceanography* **24**.

Sexton P. F., Wilson P. A. and Norris R. D. (2006a) Testing the Cenozoic multisite composite $\delta^{18}O$ and $\delta^{13}C$ curves: New monospecific Eocene records from a single locality, Demerara Rise (Ocean Drilling Program Leg 207). *Paleoceanography* **21**.

Sexton P. F., Wilson P. A. and Pearson P. N. (2006b) Microstructural and geochemical perspectives on planktic foraminiferal preservation: "Glassy" versus "Frosty". *Geochem. Geophys. Geosyst.* **7**.

Sexton P. F., Wilson P. A. and Pearson P. N. (2006c) Palaeoecology of late middle Eocene planktic foraminifera and evolutionary implications. *Mar. Micropaleontol.* **60**, 1–16.

Shenton B. J., Grossman E. L., Passey B. H., Henkes G. A., Becker T. P., Laya J. C., Perez-Huerta A., Becker S. P. and Lawson M. (2015) Clumped isotope thermometry in deeply buried sedimentary carbonates: The effects of bond reordering and recrystallization. *Geol. Soc. Am. Bull.* **127**, 1036–1051.

Stolper D. A., Eiler J. M. and Higgins J. A. (2018) Modeling the effects of diagenesis on carbonate clumped-isotope values in deep- and shallow-water settings. *Geochim. Cosmochim. Acta* **227**, 264–291.

Thiagarajan N., Adkins J. and Eiler J. M. (2011) Carbonate clumped isotope thermometry of deep-sea corals and implications for vital effects. *Geochim. Cosmochim. Acta* **75**, 4416–4425.

Torsvik T. H., Van der Voo R., Preeden U., Mac Niocaill C., Steinberger B., Doubrovine P. V., van Hinsbergen D. J. J., Domeier M., Gaina C., Tohver E., Meert J. G., McCausland P. J. A. and Cocks L. R. M. (2012) Phanerozoic polar wander, palaeogeography and dynamics. *Earth Sci. Rev.* **114**, 325–368.

Tripati, A., Vollmer, T., Perez-Huerta, A., 2017. A Quantitative Solution for the 'Cool Tropics' Paradox of Past Greenhouse Climates: Testing Diagenetic Hypotheses Combining Clumped Isotope and Electron Backscatter Diffraction Data on Foraminifera Goldschmidt Abstracts 3992.

Tripati A. K., Delaney M. L., Zachos J. C., Anderson L. D., Kelly D. C. and Elderfield H. (2003) Tropical sea-surface temperature reconstruction for the early Paleogene using Mg/Ca ratios of planktonic foraminifera. *Paleoceanography* **18**.

Tripati A. K., Eagle R. A., Thiagarajan N., Gagnon A. C., Bauch H., Halloran P. R. and Eiler J. M. (2010) ^{13}C–^{18}O isotope signatures and 'clumped isotope' thermometry in foraminifera and coccoliths. *Geochim. Cosmochim. Acta* **74**, 5697–5717.

Tucholke, B.E., Vogt, P.R., 1979. Western North Atlantic: sedimentary evolution and aspects of tectonic history. In: Tucholke, B.E., Vogt, P.R., et al., Init. Repts. DSDP, 43: Washington, DC (U.S. Govt. Printing Office), pp. 791–825.

van Hinsbergen D. J. J., de Groot L. V., van Schaik S. J., Spakman W., Bijl P. K., Sluijs A., Langereis C. G. and Brinkhuis H. (2015) A paleolatitude calculator for paleoclimate studies. *PLoS ONE* **10**, 1–21.

Vandenberghe N., Hilgen F. J., Speijer R. P., Ogg J. G., Gradstein F. M., Hammer O., Hollis C. J. and Hooker J. J. (2012) Chapter 28 – The Paleogene Period. In *The Geologic Time Scale* (eds. F. M. Gradstein, J. G. Ogg, M. D. Schmitz and G. M. Ogg). Elsevier, Boston, pp. 855–921.

Voigt J., Hathorne E. C., Frank M. and Holbourn A. (2016) Minimal influence of recrystallization on middle Miocene benthic foraminiferal stable isotope stratigraphy in the eastern equatorial Pacific. *Paleoceanography* **31**, 98–114.

Watkins J. M., Hunt J. D., Ryerson F. J. and DePaolo D. J. (2014) The influence of temperature, pH, and growth rate on the $\delta^{18}O$ composition of inorganically precipitated calcite. *Earth Planet. Sci. Lett.* **404**, 332–343.

Watkins J. M., Nielsen L. C., Ryerson F. J. and DePaolo D. J. (2013) The influence of kinetics on the oxygen isotope composition of calcium carbonate. *Earth Planet. Sci. Lett.* **375**, 349–360.

Westerhold T. and Röhl U. (2013) Orbital pacing of Eocene climate during the Middle Eocene Climate Optimum and the chron C19r event: Missing link found in the tropical western Atlantic. *Geochem. Geophys. Geosyst.* **14**, 4811–4825.

Westerhold T., Röhl U., Frederichs T., Bohaty S. M. and Zachos J. C. (2015) Astronomical calibration of the geological timescale: closing the middle Eocene gap. *Clim. Past* **11**, 1181–1195.

Wilson P. A. and Opdyke B. N. (1996) Equatorial sea-surface temperatures for the Maastrichtian revealed through remarkable preservation of metastable carbonate. *Geology* **24**, 555–558.

Zachos J. C., Dickens G. R. and Zeebe R. E. (2008) An early Cenozoic perspective on greenhouse warming and carbon-cycle dynamics. *Nature* **451**, 279–283.

Zachos, J.C., Kroon, D., Blum, P. and the Expedition 208 Scientists (2004) Site 1263, Proceedings of the Ocean Drilling Program, Initial Reports Volume 208, pp. 1–87.

Zachos J. C., Pagani M., Sloan L., Thomas E. and Billups K. (2001) Trends, rhythms, and aberrations in global climate 65 Ma to present. *Science* **292**, 686–693.

Zachos J. C., Stott L. D. and Lohmann K. C. (1994) Evolution of Early Cenozoic Marine Temperatures. *Paleoceanography* **9**, 353–387.

Associate editor: Jay Quade